19 Apatite Luminescence

Glenn A. Waychunas

E.O. Lawrence Berkeley National Laboratory
Earth Science Division MS 70-108B
1 Cyclotron Road
Berkeley, California 94720

INTRODUCTION

Apatite group minerals are among the most interesting of luminescent minerals due to their wonderful combinations of varying emission color, complex zoning, and intriguing associations. Several of the most famous mineral localities known for spectacularly fluorescent mineral associations involve apatite group minerals, calcite and ore minerals. For example, Långban, Sweden, with svabite, hedyphane and mimetite; and Franklin, New Jersey, USA, with fluorapatite, svabite and turneaurite (see e.g., Bostwick 1977, Robbins 1994). Apatite is also an extremely common mineral, formed under a wide range of conditions and in many types of host rock. The diversity of its luminescence is created in part by (1) the ability of the apatite structure to incorporate transition metal, REE and anion impurity activators and co-activators, often in combination; (2) the varying types of associations and formation conditions that promote luminescence activity; and (3) the nature of the structure of the apatite host itself. This favorable and flexible host structure has not been lost to commercial enterprises, as apatites have long been used as synthetic phosphors in industrial and consumer products, and more recently as laser matrix materials. Because the luminescence is often associated with rare earth elements (REE), apatite is frequently useful as a REE-indicator mineral. Indeed, apatite can act as a reservoir for REE, making fractionation and isotopic analyses feasible. Analysis of the REE content can also serve as an indicator of growth rate, growth conditions, local chemical mixing and redox conditions. As apatite is readily stimulated to luminescence by an electron beam, cathodoluminescence is frequently reported and contributes to trace contaminant REE analysis, and characterization of chemical zoning.

The thermo-luminescence of apatite has also been studied with an aim to extract details of the defect electronic structure. As bone and teeth materials have hydroxyl-apatite as their main mineral component, it would seem that thermoluminescence could be used to determine age and thermal history of fossil material. Even in meteorites, where apatite is rare, thermoluminescence has been used to investigate resetting and equilibration temperatures (McKeever 1985). Most detailed studies of the physics of apatite luminescence have been done on particular synthetic compositions, but a number of surveys are also available that describe the spectra of suites of natural samples (Gaft et al. 2001a, Gorobets 1968, 1981; Knutson et al. 1985, Lapraz and Baumer 1983, Kempe and Götze 2002, Marshall 1988, Mitchell et al. 1997, Panczer et al. 1998, Portnov and Gorobets 1969, Reisfeld et al. 1996, Remond et al. 1992, Roeder et al. 1987, Taraschan 1978). In the discussion herein the luminescence results from both natural and synthetic apatites have been combined to best summarize the current state of knowledge. Although the coverage of apatite group mineral compositions considered is not intended to be exhaustive, especially as the literature is heavily biased in favor of fluorapatite compositions, efforts have been made to include information of use to petrologists, geochemists, materials scientists, ceramists, and mineral collectors.

Studies of luminescence in apatite have not been widely used in geochemistry or mineralogy to date, a situation that the author believes is due (paradoxically) to the great

1529-6466/00/0048-0019$05.00 DOI: 10.2138/rmg.2002.48.19

sensitivity of luminescence phenomena, which respond to any slight change in the nature of the valence electrons and their accessible electronic states. This has made spectral interpretation difficult for natural minerals, and requires that most studies utilize models with simplified chemistry. Luminescence processes can also involve several species in a structure and multiple energy transfer processes, so that amplitude information (and thus quantitative concentration or occupation information) can be difficult, if not impossible, to model. However such problems are mitigated by the potential information available on many types of electronic processes, and by the extremely low measurement thresholds afforded by emission spectroscopy techniques, laser excitation, and photon counting detection systems. Further, pulsed and gated spectroscopy techniques are enabling separation of electronic processes as never previously possible, thus opening the door to electronic characterization of natural materials that are heterogeneous on multiple levels (types of sites, surfaces, defects, substituents, traps, etc). Apatite group minerals are a perfect focus for luminescent studies, not only for their potential return on many aspects of geochemical processes, but also for their inherent richness of crystal chemical and petrological diversity.

DEFINITIONS

Types of luminescence

It is crucial to understand the nomenclature used for luminescence investigations, as there are important aspects not found in descriptions of optical spectroscopy, and numerous authors use terminology in somewhat different ways. The general approach here is to use terms as defined by Garlick 1958. *Fluorescence* is here taken to be the same as photoluminescence, i.e., luminescence excited by high energy visible or ultraviolet light, and created by a spin-allowed emission process. *Phosphorescence* is a term applied to spin-forbidden processes that are generally very slow compared to spin-allowed transitions. The term is usually associated with organic systems where the differences between spin-allowed and spin-forbidden transitions are very dramatic. In heavier atoms with more interacting electronic states and additional factors influencing transition probabilities, the distinction is not as clear (Blasse and Grabmaier 1994). *Thermoluminescence* (TL) is the result of the untrapping of excited electrons post-excitation. This is a separate process from phosphorescence although it also produces a delay in emission. A general term for all light emission once excitation has been removed is afterglow, which includes all emission mechanisms. *Cathodoluminescence* (CL) is the stimulation of luminescence via electron excitation, usually with an electron microprobe (EMP) or a scanning electron microscope (SEM), but other devices use low energy plasmas to produce wide-field electron and ion excited luminescence (e.g., Luminoscope). *Radioluminescence* is due to excitation from high energy photons (x-rays and gamma rays) or from high energy particles, with the latter sometimes called Ionoluminescence. *Laser-excited luminescence* is the same as photoluminescence, although the energy density applied to the sample can be orders of magnitude more than with ultraviolet sources. *Pulsed laser-excited time-resolved luminescence* involves extremely short pulses of laser light that excite luminescence whose decay rate can then be measured with high-speed spectroscopy, or alternatively, an entire spectrum can be collected after a fixed delay period or over a particular interval post-excitation. This allows separation of features in the emission spectrum on the basis of excited state lifetimes and energy transfer time (Gaft et al. 2001a,b, 1999, 1998a; Solomonov et al. 1993).

Types of luminescence spectra

The *emission spectrum* for a luminescent system is the spectrum of emitted light for

a given excitation energy or type of excitation. A given system may have large variations in the emission spectrum depending on the excitation energy and internal electronic mechanisms. The great majority of luminescence spectra in the mineralogical literature are emission spectra. The *excitation spectrum* for a luminescent system is the spectrum of exciting energy (and especially photon energy) that gives rise to a particular emission feature (i.e., photon emission energy). In general, the excitation spectrum of a luminescent spectrum must be consistent with all other excitation spectra because the final state emission level and other internal energy levels are fixed in energy (see e.g., Blasse and Grabmaier 1994, Henderson and Imbusch 1989). The *absorption spectrum* consists of the energy of radiation that is absorbed by species in the luminescent system. For UV-Vis-IR light it is identical to optical absorption spectroscopy. As with the excitation spectrum the absorption spectrum must be related directly to the spacing of fixed energy levels in the material.

Luminescence terms

A detailed description of luminescence processes is beyond the scope of this article. Readers who wish to delve further into luminescence physics and theory can find much useful information in the extensive and approachable reviews by Blasse (1988), Henderson and Imbusch (1989), Marshall (1988), and Shionoya and Yen (1999). A more mineralogical introduction to the field is given by Waychunas (1989) and references therein. Here, the bare essentials are introduced. *Activators* are substituents or impurities in materials that help to produce or aid in luminescence by acting as absorption or emission centers and often as both. Co-activators or *sensitizers* are activators that operate in pairs or groups to produce luminescence, usually with one activator absorbing energy and transferring it to the other for emission. Sometimes the host lattice can function as the absorber in a luminescent system, in which case we refer to "lattice-sensitized" luminescence. Silicate host lattices often can function as lattice-sensitizers (Blasse and Grabmaier 1994). *Quenchers* are substituents or impurities that absorb excitation energy in some manner, usually dispersing the energy as lattice vibrations, and thereby reducing luminescence activity. *Energy bands* are quasi-continuous fields of *energy levels* that an electron can occupy in a solid. They are created by the action of the Pauli exclusion principle on the atomic energy levels of identical atoms on lattice sites within crystals. Forbidden energy bands or *band gaps* are related energy level fields that cannot be occupied by any of the electrons in the crystal structure, but may have within them levels produced by impurity atoms or defects. Apatite without a large concentration of impurities is an insulator, as it has a large band gap between the (filled) valence and (empty) conduction allowed bands. Most phosphors are insulators, with activators producing energy levels in the band gap.

A second class of semi-conducting phosphors and fluorescent minerals, including sphalerite, behave differently than insulator materials, but are not considered further here. *Trapping states* are energy levels associated with impurity atoms within the band gap. These states can hold onto or trap an excited electron which can be released later via thermal stimulation. This is one of the mechanisms contributing to afterglow, and is the basis for thermoluminescence spectroscopy. The *Stokes shift* is the difference between the absorption energy and the emission energy in a luminescent system. It is usually positive due to energy losses after absorption, and thus the emission is generally at longer wavelengths than the absorption. Energy absorbed that is not released in a luminescent (or *radiative*) emission process, is said to be lost to *non-radiative electronic transitions*. Transitions between energy levels, Stokes shifts and the width of transition bands (peak or line width) are exemplified with a configurational coordinate diagram. Many of the terms defined here are illustrated with configurational coordinate diagrams in Figures 1 and 2.

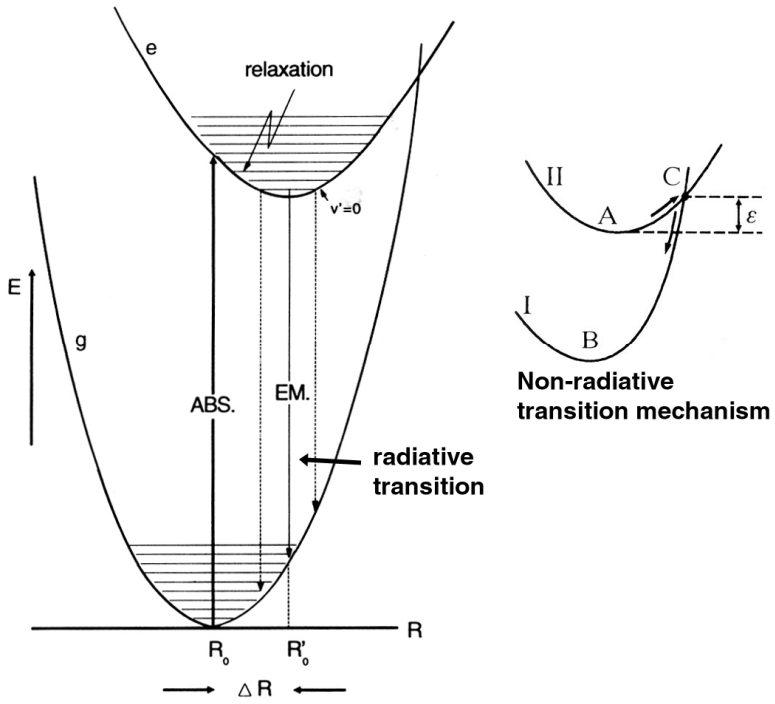

Figure 1. Configurational coordinate diagram. Each electronic state is represented as a harmonic oscillator system, with interatomic distance R on the abscissa, and energy on the ordinate. Vibrational states are represented by horizontal lines. Higher intensity vibrations result in larger R excursions in any given state. An absorption from the lowest energy state, g (for ground), takes place from the lowest vibrational level of the ground state into a higher vibrational level of the lowest excited state, e (for excited). Relaxation occurs by successive drops in the vibrational levels with loss of thermal energy as lattice phonons. Emission takes place as the electron transitions from the lowest vibrational levels of the excited state. The shift in energy between the absorption and emission transition is the Stokes shift. Differences in the curvature of the states are related to the symmetry of the state and several electrostatic factors. Transitions among similar symmetry states generally produce narrow bands, while transitions between different symmetry states give rise to large band widths. This is readily seen in divalent vs. trivalent REE spectra (see Fig. 14). The small diagram shows a non-radiative transition produced by crossing ground and excited states. If the vibrations in the excited state A are large enough to get the system to point C, no photon emission occurs. This is the main reason why increasing temperature quenches luminescence, and why vibrational states affect excited state lifetimes. Modified after Blasse and Grabmaier (1994) and Shionoya and Yen (1999).

LUMINESCENCE METHODS

Photoluminescence, cathodoluminescence and radioluminescence distinctions

Most amateur mineralogists and mineral collectors describe luminescence in minerals via response to ultraviolet (UV) light, often of several wavelengths. This characterization of the photoluminescence remains popular, and most species of luminescent minerals have been described via this method (e.g., Henkel 1989, Robbins 1994, Robbins 1983). Typical wavelengths of UV light from Hg-discharge lamps are 365, 312 and 253.7 nm, often referred to as "long wave" (LWUV), "middle wave" (MWUV) and "short wave" (SWUV), respectively. The actual emission wavelengths vary in the case of LWUV and MWUV as these are actually produced by different combinations of UV phosphors within the lamp envelopes. These wavelengths correspond to presently accepted divisions of UV called UVA, UVB and UVC,

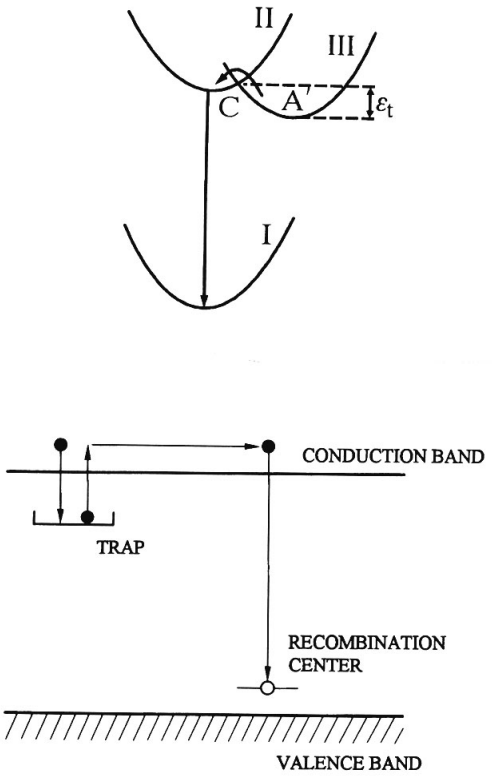

Figure 2. Thermoluminescence depicted from the configurational coordinate model (top) and from the band model (bottom). In the coordinate model the trapped electron occupies an excited state (III) slightly lower in energy than the main excited state (II). Heat can induce vibrations, which move the electron into the (II) state by direct crossover at C. A transition can then occur to the ground state (I), resulting in emission. In the band model heat moves the trapped electron to the conduction band where it can travel throughout the crystal until it recombines with a hole at the bottom of the band (forbidden energy) gap. [Used by permission of the CRC Press, from Shionoya and Yen (1999) Figs. 49 and 50, p. 90.]

respectively. Museums that display luminescent minerals often use one or more of these wavelengths in showcases. UV provides a convenient and relatively effective way of exciting visible luminescence, and the quantitative efficiency of the luminescence process can be readily measured. Laser-stimulated photoluminescence provides significantly higher energy density than Hg-discharge lamps. However, the energy density injected into a luminescent system by a Hg-UV source, and even a UV laser source is much lower than can be achieved by electron beam excitation. In cathodoluminescence (CL) excited with an SEM the electron beam is typically on the order of microns in diameter, penetrates to a few microns in depth, and can deposit up to a few mW of power into this region. A strong UV lamp, by comparison, will produce roughly a few tens of mW per centimeter diameter area with penetration of a few mm or so. Hence the CL excitation inputs some 10^9 times more energy per unit volume. This high energy density results in a cascade of x-ray emission and direct production of Auger electrons, both of which excite luminescence, plus the excitation of electron-hole pairs (Fig. 3). The net effect is greatly enhanced excitation of most luminescent processes including very inefficient ones that would not be visible or quantifiable with UV excitation. Additionally, the spatial resolution of the electron beam allows mapping of luminescent activity, which can be done in concert with chemical analysis by analysis of the x-ray emission. Such work is becoming increasingly important in geochemical studies of trace and minor elements. The only drawbacks to CL are the inability to study excitation spectra, saturation effects that produce a non-linear dependence of emission intensity with beam current, and degradation of the CL intensity with excitation time. Saturation effects can affect the apparent amplitude of peaks in the CL spectrum, and variations in the detector efficiency as a function of emission wavelength can also influence relative peak amplitudes (Barbarand and Pagel 2001) (Fig. 4). X-ray excited luminescence is intensely studied as many uses of phosphors are tied to x-ray measurements, medical fluoroscopy and

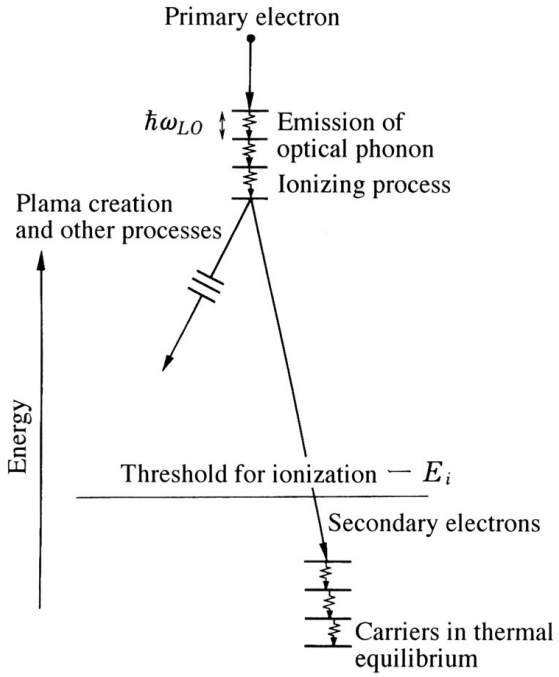

Figure 3. Cascade of effects in CL excitation. Creation of secondary electrons can lead to local bond disruption and valence changes in the sample. Hence spectra may preserve experimentally induced changes not intrinsic to the sample. Modified after Robbins (1980).

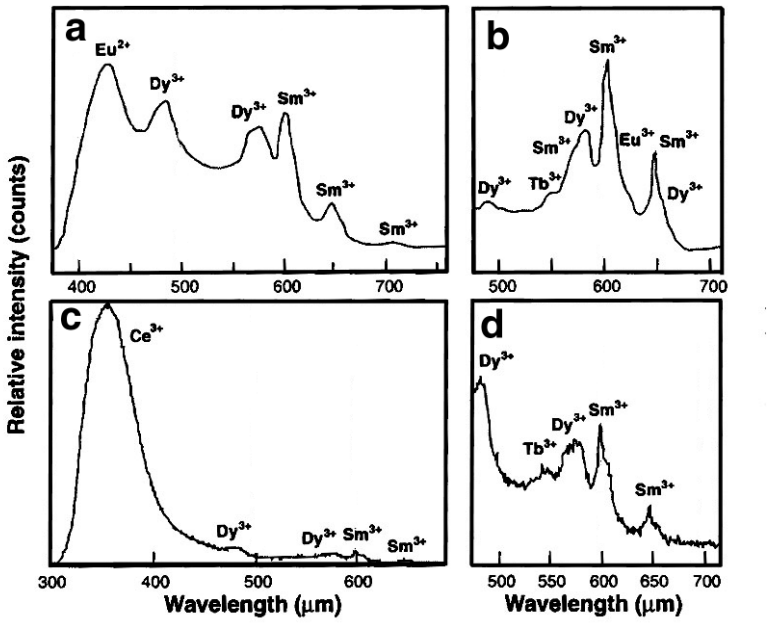

Figure 4. CL emission spectra from Durango Mexico fluorapatite reported in the literature. (a) Roeder et al. (1987). (b) Murray and Oreskes (1997). (c) and (d) Barbarand and Pagel (2001). (c) demonstrates the importance of having a detector that is sensitive to the shorter wavelength part of the spectrum. Modified after Barbarand and Pagel (2001).

radiology. However, x-ray sources suitable for the analysis of radioluminescence in mineral samples are mainly limited to synchrotrons, and hence this has been little explored. Particle-excited luminescence, generally as a byproduct of PIXE analysis, is

performed only with proton and ion accelerators (Karali et al. 2001). The energy input into the sample in this case can be even higher than the CL case, and there is frequently massive local structural damage and electron transfer that can complicate spectral interpretation.

Emission, absorption and excitation spectroscopy

Luminescence emission spectroscopy is the spectral analysis of emitted photoluminescence, cathodoluminescence or other process. It has been described briefly in Waychunas (1989) and Marfunin (1979), and in considerable detail by Henderson and Imbusch (1989). This process is the modern day analog of Newton's analysis of sunlight with a wavelength-dispersing prism, and has been around for a century. Time-resolved emission spectroscopy is a relatively new technique usually paired with pulse laser excitation. If the laser pulse is brief enough (typically a few nanoseconds), the excitation is considerably shorter than most fluorescence excited state lifetimes, offering the possibility of separating emission from different electronic states. In practice, this technique is applied by the synchronous use of laser pulses and gated detectors. One timed signal will activate the laser, while the next, after a predetermined wait, will turn on the detector. Another signal will turn off the detector after a set dwell period. In this way, over many thousands of pulses, a complete emission spectrum can be acquired from electronic states with certain lifetimes. This is of particular value when trying to sort out the emission of activators whose emission spectra heavily overlap, but differ in lifetime (Gaft et al. 1998a).

Classic absorption spectroscopy has been described in detail by Burns (1993), Rossman (1988) and many others. The key aspect that relates to luminescence is that the absorption spectrum indicates the energy level separations, i.e., the electronic structure, of the absorbing species. Once these are known, comparison with the excitation spectrum can indicate type of activator and type of sensitizer. Host lattice sensitization can also be determined in this way.

Excitation spectroscopy requires instruments with monochromators both on the incident and emission side of the sample. The emission monochromator is set to a fixed energy consistent with an emission peak, and the excitation monochromator is scanned. This produces a spectrum of all absorption states that ultimately give rise to the particular emission peak.

Apatite occurrences

Apatite is commonly found in sedimentary, metamorphic, igneous and hydrothermal rocks, and its luminescent activity and emission spectrum seem to differ with paragenesis. For example, Mariano (1988) reported that apatite found in granitic rocks and pegmatites frequently has a strong yellow to yellow-orange fluorescence and CL, while CL from apatites in carbonatites is usually blue, and that from apatites in peralkaline syenite is pink-violet. John Hanchar (pers. comm.) also reports that granitic apatites emit a bright creamy yellow CL, based on 20-25 observations. Somewhat different variations can also be seen in the emission spectra (excited by UV light) collected by Gorobets (1981) reproduced in Figure 5. These spectra are dominated by a blue component created by Ce^{3+} and Eu^{2+}, and an orange component created mainly by Mn^{2+}. Roughly equal amounts of blue and orange emission lead to a pink luminescence, and hence the dominant emission colors range from orange to pink to blue. Notable occurrences of pegmatitic apatite with strong orange-yellow luminescence are those of the granite quarries of New Hampshire and Connecticut, the quarries and mines near Spruce Pine in North Carolina, and the famous Harding mine near Taos, New Mexico. Outside the USA, brightly yellow fluorescing apatite occurs in the pegmatites of the

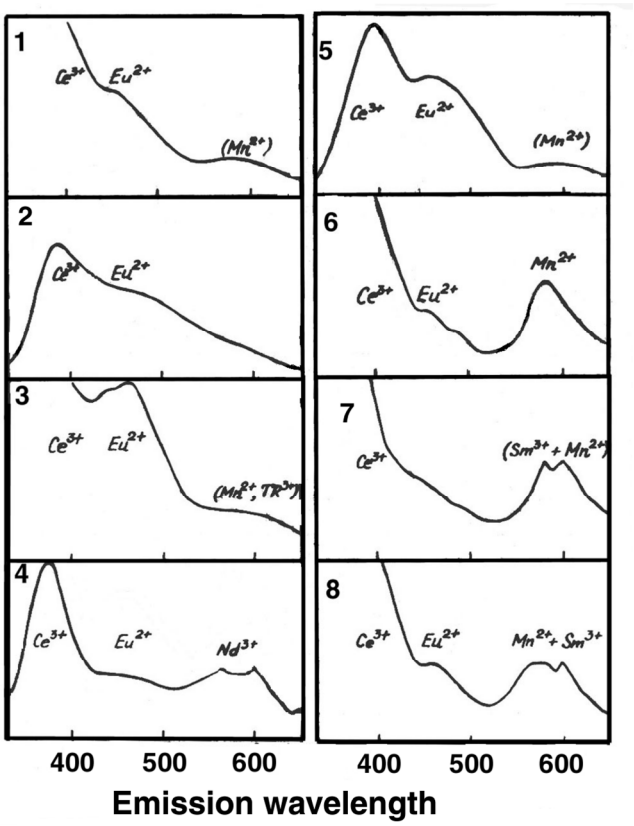

Figure 5. UV-excited emission spectra for apatite from different geological environments.

(Modified after Gorobets 1981.)

1-kimberlite.

2-carbonatite.

3-urtite (Khibiny).

4-nepheline syenite (Lovozero)

5-gabbro

6-diorite

7-granodiorite

8-granodiorite.

9-granitic pegmatite.

10-plutonic pegmatite.

11-ultramafic skarn.

12-greisen with two generations of apatite.

13-manganapite with 26% MnO.

14-high temperature calcsilicate.

15-low temperature calcsilicate.

16-calcite-phlogopite metasomatic body.

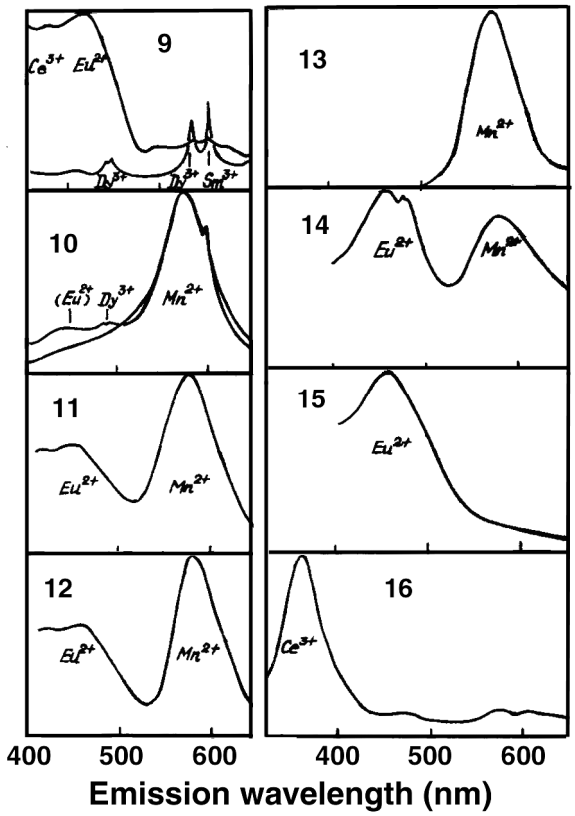

Figure 5, continued.

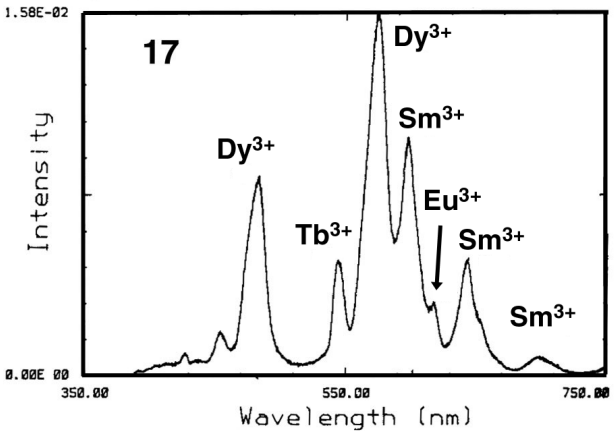

Cathodoluminescence.

17-supergene apatite from crusts on a botryooidal laterite derived from a carbonatite, Mt. Weld Western Australia.

Modified after Mariano (1989).

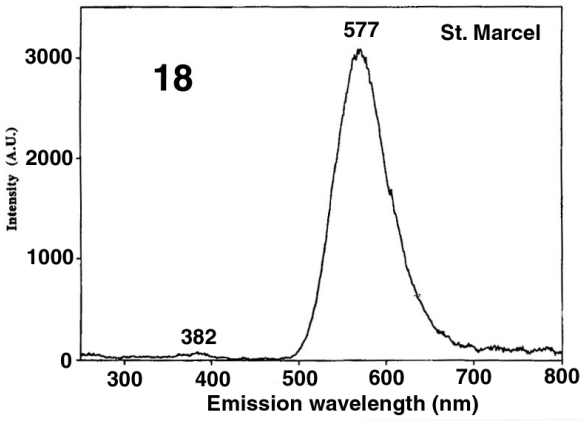

18-arsenic-containing fluorapatite from St. Marcel, Italy.

Modified after Perseil et al. (2000).

Minas Gerais region of Brazil, and in the gem pegmatites of the mountainous regions of Pakistan and Afghanistan (Robbins 1994). Occasionally, pockets in the pegmatites allow for the development of spectacular euhedral apatite crystals from colorless to light pink in color and with spectacular bright yellow photoluminescence. However, pegmatitic apatites do not always yield yellow-orange emission, and blue, pink-violet, and orange-red emission are also observed.

Magnetite ore apatites. Apatite is common in hydrothermal iron ore deposits such as at the Cerro de Mercado mine in Durango, Mexico, in southwestern Utah, in the Grenville formation at Mineville, New York, and in the Atlas mountains of Morocco. In all of these deposits, fluorapatite is found as substantial pods of intersecting crystals, and sometimes as the dominant rock-forming mineral. The iron ore acts to selectively partition Fe, Ni and other transition metals, leaving the rare earths to the fluorapatite. Accordingly, iron deposit fluorapatites display some of the most spectacular rare-earth-activated luminescence. In general these apatites are all rich in F and display blue-violet emission under SWUV, and a somewhat more violet-pink emission under MWUV. CL emission is generally bright blue-violet. As we shall see below, this emission is consistent with domination by Eu^{2+} and Ce^{3+} activation.

Other ore deposits. The classic fluorapatite specimens and fluorescent specimens are associated with these localities, notably Långban Sweden (ores of Mn, Fe, As), Franklin NJ (Zn), Panasqueria Portugal (Sn, W), and Llallagua, Bolivia (Sn, W). These ore bodies are mainly hydrothermal in origin, but in the case of Franklin multiple alteration events have created unusual species and chemistry. The Långban apatite group minerals are

largely svabite and related lead and arsenate apatites such as hedyphane and mimetite. Most of the Långban apatites fluoresce in shades of yellow to reddish-orange, and the author has not seen pink-violet or blue emission in any apatites from this mine in examining hundreds of specimens. This type of emission suggests mainly Mn^{2+} activation and a relative paucity of REE. However at the smaller Jacobsberg mine in Sweden, a similar ore body, johnbaumite has a distinctly pink-violet emission, which must be due to significant REE activation. At Franklin, fluorapatite is common but turneaurite, svabite, johnbaumite and other apatite group minerals are found occasionally, with most material showing strong luminescence. Most of the fluorescent emission is orange, with relatively slight variations in specimens seen by the author, suggesting Mn^{2+} activation with little REE contributions. At Panasqueria the fluorapatites can vary in luminescent intensity from nonluminescent to exceptionally strong. The crystals can also display spectacular luminescence zoning, typically with the bodies of the crystals fluorescing yellow, and the ends blue (Fig. 6, Color Plate 8), but other combinations and emission colors are also observed.

Figure 6. Figure 6 contains Color Plates 5-16. They are located in the color signature in this chapter.

Marbles and carbonatites. Fluorapatites are commonly found in marble deposits such as the region around the Franklin ore body, and the marbles associated with skarns in the Bancroft and Wilberforce areas of Ontario, Canada. The Canadian fluorapatites usually have intense physical color which varies from a pale green to a dark green or a reddish brown. In general, the pale specimens have the strongest luminescence under UV, but most will show a blue to gray emission under SWUV or MWUV. CL response is generally a bright blue. Some of the most spectacular specimens came from the Silver Crater mine near Bancroft, where individual crystals weighing 10 kg were found by the author. Such crystals exhibit both Mn^{2+} and REE activation, including contributions from Eu^{2+}, Ce^{3+}, Dy^{3+}, Sm^{3+} and Eu^{3+}. Carbonatites, noted above, appear to be enriched in Eu^{2+} and Ce^{3+} with low Mn^{2+}. This yields an interesting difference in coloration between CL and UV excitation, as CL excites the Eu and Ce efficiently producing a strong blue emission, but the UV excitation energy is transferred to the Mn^{2+} so that the photoluminescence is usually a deep red or pinkish-red.

Sedimentary and biologic apatites. Diagenetically-produced sedimentary apatites show generally weak luminescence, though spectral analysis has been done to reveal the presence of REE and Mn. Fossil bone material, if luminescent, appears to be activated by substituents or defects that were incorporated during diagenetic alteration. In general the fluorescence of biological apatites is weak and has not been thoroughly explored.

APATITE STRUCTURE AND TYPES OF LUMINESCENT SUBSTITUENTS

Activator sites and occupations

Ca sites. The structure of fluorapatite is described elsewhere (Hughes and Rakovan, this volume, p. 1-12). The crystal structure of REE-rich apatite has been investigated by Kalsbeek et al. (1990). Five types of sites can be occupied by activator species: the Ca1 and Ca2 sites, the P site, the halogen site, and interstitial sites. The Ca1 site has trigonal-prism topology, with additional oxygens capping the main faces of the prism to yield 9-fold coordination. The six shorter Ca-O distances (3 × 2.40 Å, 3 × 2.46 Å) form the prism, with considerably longer Ca-O distances (2.81 Å) for the three caps. The overall site symmetry is C_3. The Ca2 site has six-fold coordination by oxygen (2.44 Å average distance, but range from 2.34-2.70 Å) and one halogen neighbor at (2.31 Å) with overall symmetry C_s. Because of their size, the Ca sites can be substituted with divalent Sr, Pb and to a lesser extent Ba, Y and REE. Na is the only major single-valent substituent

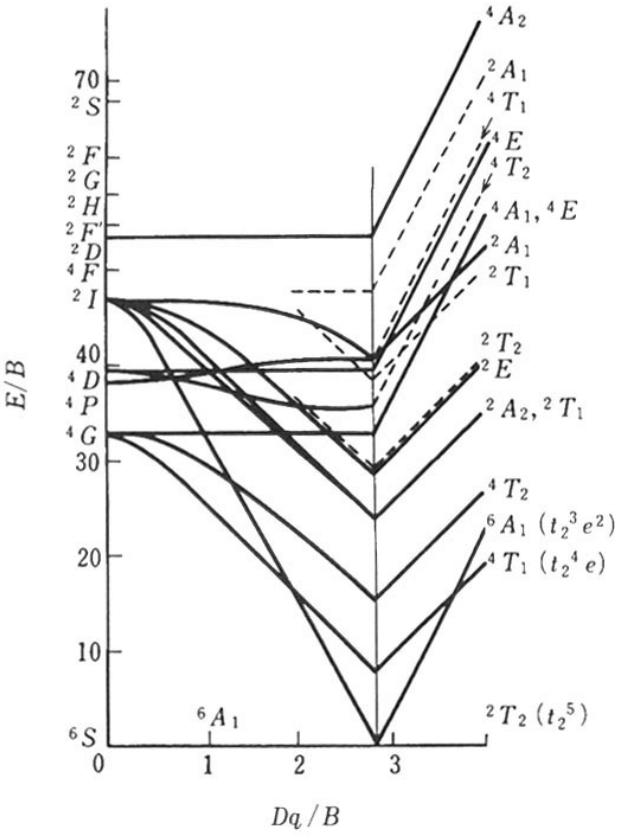

Figure 7. Tanabe-Sukano diagram for octahedral Mn^{2+} (d^5), constructed from all possible electronic states of five 3*d* electrons in an octahedral crystal field by solving the total energy as a function of the crystal (ligand) field. Pre-superscripts designate total spin state. Capital letters and subscripts designate group theory-based transformation symmetry. Such a diagram shows the relative energy placement and dependence of the possible electronic states on crystal field (Dq). For Mn^{2+} with a weak field as from oxygen, the ground state is $^6A_1$, first excited state $^4T_1$ and second excited state $^4T_2$. Increasing crystal field lowers $^4T_1$ and thus the transition energy from $^6A_1$. B is a scaling factor known as a Racah parameter. At high crystal field, Dq/B ≈ 2.8, there is a ground state symmetry change due to electron pairing (high spin to low spin transition). Note that the symmetry of the Ca1 site in apatite is not octahedal, and the diagram is even less applicable for the Ca2 site. However the concepts are generally applicable. Note also that for some state symmetries transitions between states increase in energy with crystal field strength. For details on these diagrams see Cotton (1971) and Cotton and Wilkinson (1980).

found in natural samples. Pb^{2+} is a strong absorber of UV light, and can act as a powerful co-activator for luminescence (Botden and Kröger 1948). Pb, Sr and Ba substitution for Ca will expand the apatite lattice, and this would be expected to weaken the crystal field of activator ions in other Ca sites. Such expansion usually produces a shift in the luminescence emission toward higher energies because the weaker crystal field will result in a higher energy for the lowest excited state, and this increases the energy separation between the ground and the lowest excited state—($^6A_1$) and ($^4T_1$) states, respectively, for Mn^{2+} in an octahedrally coordinated site (Fig. 7). Such a change is observed in synthetic Sr and Ba apatite phosphors (Shionoya and Yen 1999). Sr preferentially occupies the Ca2 site (Rakovan and Hughes 2000), and it is probable that Pb^{2+} and Ba^{2+} also prefer the Ca2 site. Pb^{2+} is ordered into this site in hedyphane, but ordered Ba-Ca or Ba-Sr apatites have apparently been little studied. Other common substituents are Mn^{2+} and to a much lesser extent, Fe^{2+}. Interestingly, the apatite structure preferentially takes up Mn^{2+} over any of the other 3*d* transition metal ions. As Mn^{2+} is an activator of luminescence, and Cu^{+}, Ni^{2+} and Fe^{3+} strongly quench Mn^{2+} emission, this partially explains the frequent luminescence of natural apatites. The site partitioning of Mn^{2+} remains disputed, although most studies indicate that there is a preference for the Ca1 site. X-ray diffraction structural refinements indicate a Ca1 site preference that decreases with increasing Mn^{2+} (Hughes et al. 1991a, Suitch et al. 1985). Synthetic fluorapatites used in phosphors also have Mn^{2+} partitioned into Ca1 (Ryan et al. 1970, 1971). In contrast, EPR spectroscopy has indicated Mn^{2+} occupying both of the Ca sites (Warren 1970), with variations in partitioning in the Sr analogs (Ryan et al. 1972). Laser-excited photoluminescence study of the Mn^{2+} emission band in a natural fluorapatite shows that two Gaussian peaks are necessary to fit the band, and further that two relaxation times are needed to fit the emission decay profile (Gaft et al. 1997b). The larger band and relaxation component can be attributed to Mn^{2+} in the Ca1 site with a Ca1/Ca2 site occupation ratio of about 2.5:1

(Fig. 8). This component has a longer wavelength emission and a slower relaxation rate, both consistent with a stronger crystal field (Stefanos et al. 2000, Blasse and Grabmaier 1994). Trivalent lanthanides substituting for Ca require a coupled substitution for charge balance. This can be OH for O or F,Cl for O ions local to the substituted Ca site (Chen et al., 2002a). More common substitutions are SiO_4 for PO_4 and Na for a second Ca (Ronsbo 1989, Hughes et al. 1991). The trivalent lanthanides are selectively partitioned into the Ca2 site in fluorapatite, but with site ratio decreasing over the 4*f* series (Fleet and Pan 1995a,b; Hughes et al. 1991b, Mackie and Young 1973), and subject to the dependency of the apatite structure on the presence of multiple REE (Fleet and Pan 1997a,b). Sr has a stronger site preference for Ca2 than do the trivalent rare earths, and thus will displace them into the Ca1 site if present (Rakovan and Hughes 2000).

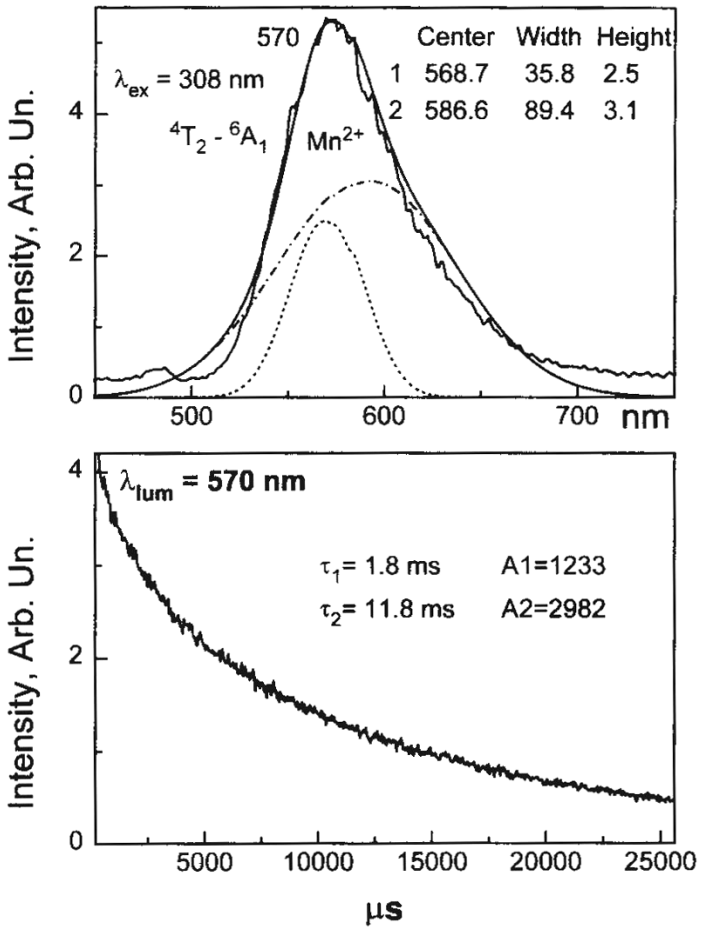

Figure 8. Mn^{2+} laser-excited emission spectrum from fluorapatite. Top: showing a possible fit for the two Ca site contributions. Bottom: Fitting to the excited state lifetime requires two components for a good fit. The components lifetimes are consistent with the symmetries of the two sites (and states). Modified after Gaft et al. (1997b).

The phosphate site. The phosphate site is highly regular and can be substituted by vanadate, chromate, arsenate, carbonate, silicate and sulfate, but only vanadate, arsenate and carbonate solid solution is widespread in natural apatites. Charge-coupled substitution schemes to aid incorporation involve the substitution of silicate for phosphate and REE^{3+} for Ca, and carbonate or sulfate for phosphate and Na for Ca. Numerous oxyanions may act as activators and sensitizers, with the most widespead being molybdate and tungstate, but vanadate and niobate can also activate luminescence (Blasse and Grabmaier 1994). Silicate is a strong absorber of UV radiation and can serve as a

sensitizer for other activators. Unfortunately the activation of apatite group minerals via these oxyanions has been little explored. Substitution of arsenate for phosphate does however have a significant effect on the apatite group minerals lattice constants, and this should translate into changes in activator crystal fields. For example, svabite has cell constants of a = 9.750 Å c = 6.920 Å while fluorapatite has typical cell constants of a = 9.367 Å c = 6.884 Å, and synthetic $Ca_5[AsO_4]_3Cl$ has a = 10.076 Å and c = 6.807 Å compared to chlorapatite with a = 9.5979Å and c = 6.7762 Å. This should produce a weakened crystal field at the Ca sites as arsenate content is increased, shifting the emission spectrum to shorter wavelengths. Another possible occupant of the P site in apatite is Mn^{5+}. Gaft et al. (1997b) showed that some natural fluorapatites demonstrate the strong IR emission bands and diagnostic luminescence decay times characteristic of Mn^{5+} doped into the P site in synthetic apatite (Moncorge et al. 1994, Oetliker et al. 1994, Scott et al. 1997). Emission spectra at two temperatures are shown in Figure 9. Oetliker et al. (1994) showed that lattice expansion when arsenate and vanadate replaced phosphate in Sr and Ba synthetic apatites reduced the MnO_4 crystal field, resulted in both a shift of emission and excitation bands, and a change in luminescence lifetime. By comparing Mn^{5+} spectra in a variety of host lattices, Oetliker et al. (1994) also determined that distortions of the MnO_4 tetrahedron had greater effect on luminescence lifetime and temperature quenching than cell dimension changes. Mn^{5+} also produces absorption bands at 540 and 660 nm in tetrahedral coordination and is partially responsible for the coloring of blue and blue-green fluorapatites.

The halogen site. The halogen site may contain F, Cl, Br or OH though Br in significant levels is found only in synthetic apatites. None of these species act as activators or sensitizers, but they can contribute to cell dimension changes and thus

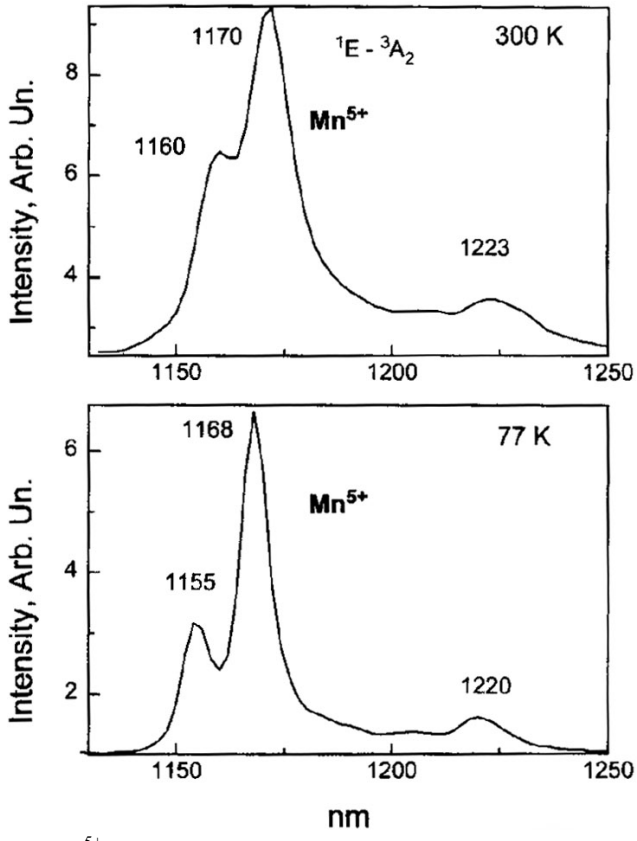

Figure 9. Mn^{5+} in P site emission spectra. Note the improved resolution at lower temperature. Modified after Gaft et al. (1997b).

activator crystal fields. By far the largest effect is due to substitution of Cl for F or OH. Compare fluorapatite with chlorapatite above, and also the synthetic varieties of pyromorphite:

$Pb_5[PO_4]_3Cl$	a = 10.976 Å	c = 7.351 Å
$Pb_5[PO_4]_3F$	a = 9.760 Å	c = 7.30 Å
$Pb_5[PO_4]_3OH$	a = 9.774 Å	c = 7.291 Å

These values indicate that Cl should have a definite effect on activator crystal fields, and one would expect a priori that the increased cell should result in a smaller field at the Mn site and an emission shift to shorter wavelengths. In fact, what is observed is a shift to longer wavelengths (Ryan et al. 1971; Fig. 10). The substitution of Cl^- for F^- has a large effect on the Stokes shift but little effect on the excitation spectrum of the Mn^{2+}. This suggests that the Cl^- is changing the energy configuration of the Mn^{2+} excited state possibly due to Ca2 site distortion (Ryan et al. 1971).

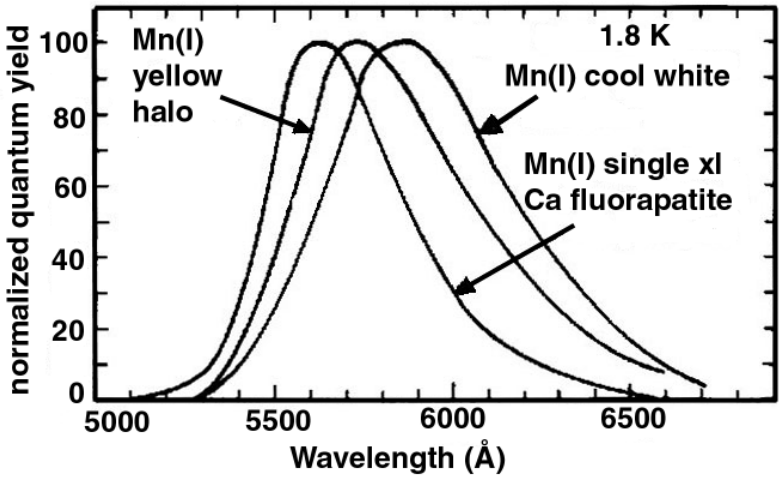

Figure 10. Changes in Mn emission (from Mn in Ca1 site) from fluorapatite with changes in other substituents. "Yellow Halo" synthetic fluorapatite has Sb and Cd added. "Cool white" has Sb, Cd and Cl added. The cool white composition should have increased cell dimensions, and thus a smaller crystal field. Ordinarily this should raise the energy of the emission. Modified from Ryan and Vodoklys (1971).

Defect sites. Besides lattice defects such as dislocations and stacking faults, vacancies can be created in the apatite structure by certain types of impurity substitutions. For example, two REE^{3+} can substitute for three Ca ions, creating a Ca vacancy (Fleet and Pan 1994), or a halogen can be lost in order to satisfy the charge of a silicate group substituting for phosphate. Anion vacancies can serve as sites for electron centers, such as F (from the German "farbe") centers. The pink color of pegmatitic fluorapatites (Marfunin 1979) is due to the F center formed from a fluorine vacancy with a trapped electron. Other defect sites are associated with molecular groups which do not readily fit into the apatite structure. One such species is the uranyl group, UO_2^{2+}, a linear ion with very strong luminescence, which has been observed in sedimentary apatite luminescence (Panczer et al. 1998). Other defect sites in apatite can act as traps for electrons or holes, and give rise to thermoluminescence-phosphorescence effects. One such trapping site can be produced by cation or anion vacancies. Chen et al. (2002b) suggested that two Gd^{3+} ions can substitute at adjacent apatite Ca1 sites with a neighboring Ca2 site vacancy, forming a trimer defect unit. This mechanism could possibly be used by other trivalent REE. The cation vacancy would have a net negative charge and could thus trap holes, leading to thermoluminescence behavior.

APATITE ELECTRONIC STRUCTURE

Band structure

The fluorapatite electronic structure is typical of a low conductivity insulator with a significant energy gap between the valence and conduction bands (Louis-Achille et al. 2000, Blasse and Grabmaier 1994). The energy gap of about 8 eV requires photons of wavelength near 1500 Å to create carriers, so that lattice UV absorption is unimportant for Ca apatites, i.e., the relevant absorption that excites any activators occurs at the activator or sensitizer sites themselves, which are located in the band gap. The case is entirely different for CL, where much greater energies are available for excitation, as well as much higher excitation densities. Hence, pure Mn^{2+} doped fluorapatites will hardly show any luminescence under ordinary UV excitation, but will emit brightly under the electron or ion beam. The situation changes for the Pb apatites, where strong absorption of short wave UV occurs, and the energy can be transferred to the Mn^{2+} to excite luminescence. This particular case has apparently not been studied in detail during phosphor research, as Pb-sensitized halophosphate phosphors are either not as efficient as compositions having other sensitizers, or because of deterioration with time in applications. Hence the action of Pb^{2+} as a sensitizer is drawn by analogy with the Pb^{2+}-Mn^{2+} system in calcite and wollastonite (Shionoya and Yen 1999, Leverenz 1968). Ce^{3+} and Sb^{3+} are other sensitizers that transfer excitation energy to Mn^{2+} and have been thoroughly explored due to phosphor research (Shinoya and Yen 1999).

Spectra of Mn^{2+} in the Ca sites. An approximate calculation for crystal field splitting of Mn^{2+} 3*d* states in the Ca1 site of fluorapatite has been done by Narita (1961, 1963). According to this model, a 2% isotropic lattice contraction is expected to produce a shift of 1200 cm^{-1}, equal to an emission wavelength change from 580 nm to 620 nm (yellow to reddish-orange). The calculation shows acceptable agreement with experimental observations for the replacement of about 10% of the Ca in Ca fluorapatite by Cd. This decreases the unit cell dimensions by 0.042% and 0.35% on the *a*- and *c*-axes, respectively, and creates a shift in the emission spectral peak to longer wavelengths of about 100 cm^{-1}. The electronic structure of Mn^{2+} in fluorapatite has been measured in detail by Ryan et al. (1970, 1971). Excitation spectra obtained at 1.8 K show fine structure that can be separated into contributions from both the Mn^{2+} in Ca1 and the Mn^{2+} in Ca2 (Fig. 11). Given slightly different excitation spectra for each site, it was then possible to excite the Mn^{2+} in each site separately (Fig. 12), demonstrating the effect of the less symmetric crystal field in the Ca2 site, namely, an emission shift of 10 nm from

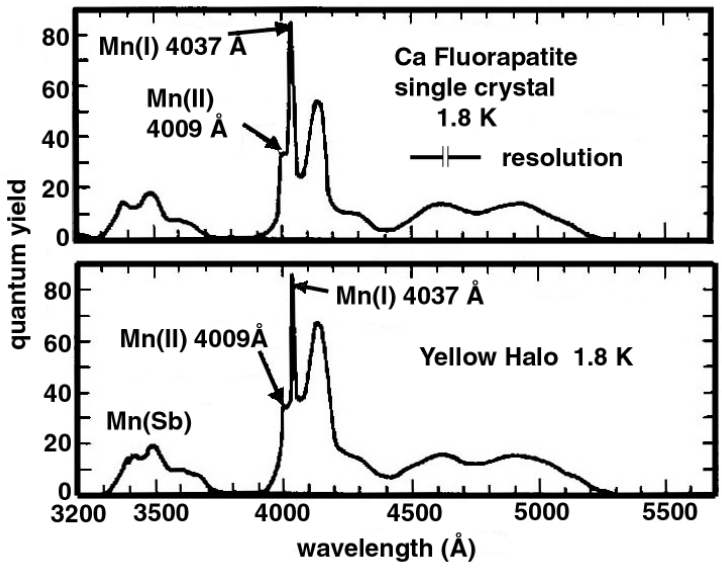

Figure 11. Excitation spectra for two of the synthetic samples depicted in Figure 10. At low temperature the Mn bands due to the two Ca sites can be separated. Modified after Ryan and Vodoklys (1971).

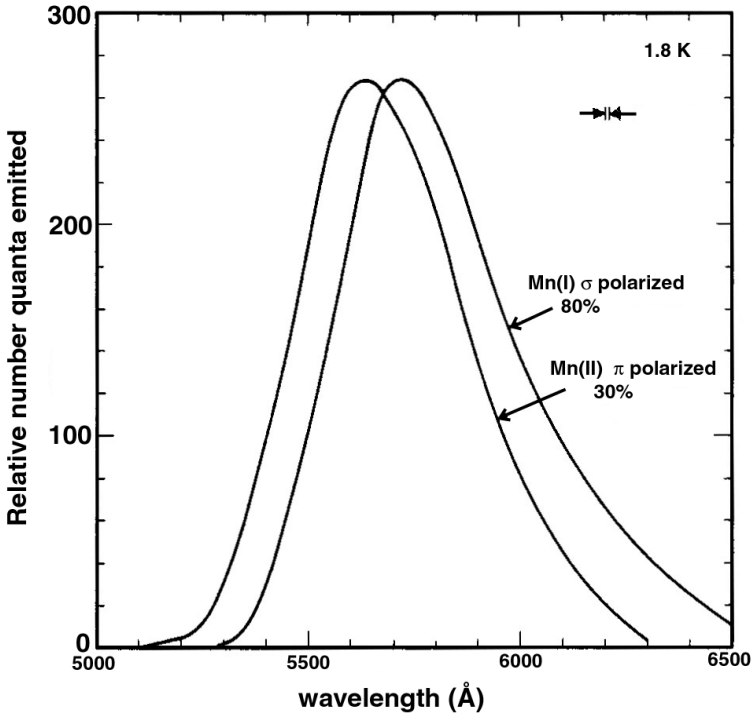

Figure 12. Separate emission spectra for Mn^{2+} in the two Ca sites in synthetic single crystal fluorapatite. Generated by taking advantage of the separate excitation bands for the sites shown in Figure 11. Compare with Figure 8. Modified after Ryan et al. (1970).

572 to 562 nm at 1.8 K. This means that the lowest excited state of the Mn^{2+} ion in the Ca2 site is about 300 cm^{-1} higher in energy than the analogous state for Mn^{2+} in the Ca1 site, consistent with a weaker crystal field at the Ca2 site.

The emission band for Mn^{2+} in apatite is always broad due to the different symmetries of the ground and excited states (Fig. 1). The band peaks at about 570 nm (yellow or yellow-orange) in fluorapatite (Gaft et al. 1997b) at room temperature excited by a UV laser. Cathodoluminescence studies (Perseil et al. 2000, Barbarand and Pagel 2001) of fluorapatites show a strong Mn^{2+} emission band at 577 nm. Asymmetry in the band has been attributed to contributions from both Ca sites which have slightly different crystal field parameters (Gaft et al. 1997b) , but the work of Ryan et al. (1970) shows that even the emission from only one of the Ca sites has asymmetry. Both studies agree on the sense of the crystal field and emission wavelength change between the two sites. The survey by Gorobets (1981) shows Mn^{2+} bands which vary between 560 and 590 nm in natural apatites, presumably due to changes in lattice parameters and Ca1 vs. Ca2 site occupation. Anecdotal evidence for the dependence of Mn^{2+} emission on composition comes from Henkel (1989) and Robbins (1994) and observations collected by the author for several dozen apatite specimens excited by UV (unpublished). Svabite from Långban, Sweden is a well characterized arsenate apatite with strong orange emission. In contrast, mimetite from Långban, Sweden has a bright yellow emission, similar to pegmatitic fluorapatites from Afghanistan and Pakistan, and from the Harding pegmatite in Dixon, New Mexico. The larger size of the mimetite unit cell is consistent with smaller crystal fields at the Mn^{2+} sites, and thus shorter wavelength emission, i.e., a shift from orange toward yellow. However the fluorapatites from the Afghanistan and Pakistan pegmatites appear to contradict this conclusion, unless the emission is dominated by REE activation. Interpretation of visual apatite emission colors are subject to large variations depending on several factors: filter effect of the physical color of the apatite, the amount and type of room lighting, and the nature of the excitation source in UV excitation. Thus, for example, physically green apatites with Mn^{2+} activation appear to emit yellow-green light due to filtering. In CL studies the spectral peaks observed are not subject to shifts due to

these factors, but large differences in intensity, background and resolution are often observed for nominally very similar material.

Luminescence intensity and quenching. There is disagreement in the literature as to whether the luminescence intensity is related to the Mn^{2+} concentration, the presence of certain quenching agents, or the presence of particular sensitizers. For example, Perseil et al. (2000) found that in fluorapatites from one location the fluorescence emission intensity was correlated with Mn^{2+}, and partially quenched by higher concentrations of arsenate substituting for phosphate. This is remarkable, as pure arsenate apatites are known to be highly fluorescent (svabite and johnbaumite) due to Mn^{2+} emission. In contrast, Knutson et al. (1985) used statistical analysis to show that fluorapatites from Panasqueira, Portugal have fluorescence not strongly correlated with Mn^{2+} content, but more with coexistence of Mn^{2+} and sensitizing REE Eu^{2+} and Ce^{3+}. Ce^{3+} and other REE are well known to be sensitizers for Mn^{2+} in other minerals, notably calcite (Blasse and Aguilar 1984). Garcia and Sibley (1988) showed that Eu^{2+} acts as a coactivator for Mn^{2+} in synthetic fluoroperovskite. Further, Chenot et al. (1981) found that Ce^{3+} and Mn^{2+} can act as coactivators in synthetic fluorapatite phosphors.

Fe^{2+} in the Ca sites has been shown to quench the Mn^{2+} emission in apatite from studies of synthetic carbonate apatite (Filippeli and Delaney 1993). The manner in which Fe^{2+} affects fluorescence varies both with total Fe^{2+} concentration and with the Mn/Fe ratio. This is entirely consistent with local quenching effects of the Fe^{2+} impurity. At low Mn and Fe concentrations, most Mn will be unaffected by exchange of energy to a nearby Fe. However at high Fe content all Mn will be affected. The range of quenching effects depends on the type of interaction between quenching ion and activator. Magnetic and electric dipole interactions are relatively short range. However, some quenching ions operate by having their own absorption bands overlap the excitation bands of the activators. In this case quenching ions anywhere in a crystal can act to absorb the exciting photons before they reach an activator. A detailed study of the quenching effects of many impurities on the Mn^{2+} emission from a synthetic "warm white" calcium halophosphate phosphor ($Ca_{10}(PO_4)_6(F,Cl)_2$: Sb^{3+}, Mn^{2+}) was done by Wachtel (1958). In this study the phosphor was excited with SWUV at 2537 Å. At the 10,000 ppm level, Cu, V, Co, Cu and Fe removed essentially all luminescence, while Ni and Cr reduced luminescence intensity by over 90%. At the 1000 ppm level, these species reduced luminescence intensity by 40 to 60%.

Even if excited directly via band gap absorption or indirectly from sensitizers, Mn^{2+} can transfer some or all of its excitation energy to nearby REE ions. This is the primary reason why Mn^{2+} emission may not be observed in apatites that have significent Mn and REE impurities. Marfunin (1979) listed Nd^{3+}, Sm^{3+}, Eu^{3+} and Tm^{3+} as the main REE for sensitization by Mn^{2+}, with Sm^{3+} being the most significant recipient. However, this type of energy transfer process does not seem to have been explored in detail. A diagram that shows how a transition metal ion could transfer energy to a rare earth system is shown in Figure 13.

Spectra of rare-earths in the Ca sites. The rare earth ions have an incompletely filled 4*f* shell, which is strongly shielded from outside interactions by the surrounding filled $5s^2$ and $5p^6$ orbitals. This means that electronic transitions within the 4*f* orbitals are only weakly influenced by crystal fields and covalency effects, and thus 4*f* to 4*f* transitions for rare earths in apatite will not be distinguishable between the Ca sites. Further, the change in configurational coordinate (ΔR) between ground and excited state is small or zero, so that very narrow absorption and emission lines will be observed. 4*f* to 4*f* transitions are parity forbidden, and would be very weak if not for some mixing of other symmetry orbital character in either the ground or excited state. This is enhanced by lower

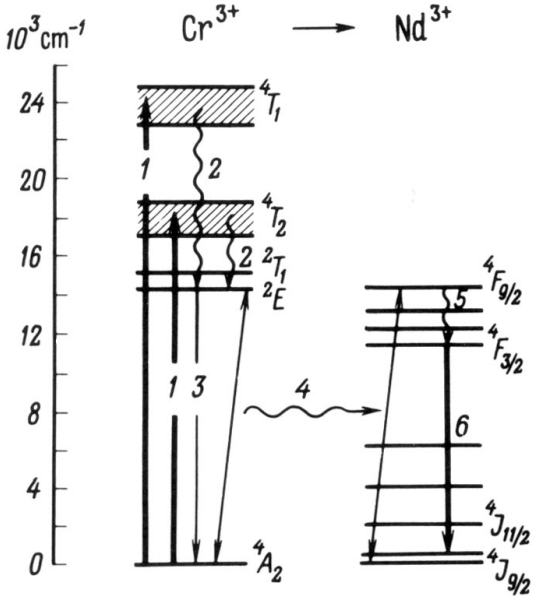

Figure 13. A scheme for energy transfer from excited Cr^{3+} to Nd^{3+}. Despite the varying transition symmetries, the energy of the two transitions shown by slanted arrows are similar enough so that there can be a coupled resonance (wiggly arrow 4) between them. This is sometimes called a "resonance radiationless transition." In this kind of diagram the curved states of the configurational coordinate plot (Fig. 1) are collapsed to show the band width in energy. Wiggly lines indicate non-radiative transitions due to the crossing of state levels and vibrational heat loss. Modified after Marfunin (1979).

symmetry crystal fields, and in this way 4*f* to 4*f* transitions will have intensity related to site symmetry. Stronger transitions that are parity allowed occur via charge transfer $4f^n$ to $4f^{n+1}\ L^{-1}$ or $4f^n$ to $4f^{n-1}$-5*d* transitions. The charge transfer transitions are strongest in rare earth ions that have a tendency for reduction, while the 4*f*-5*d* transitions are strongest in rare earths that have a tendency for oxidation. Hence the tetravalent rare earth ions (Ce^{4+}, Pr^{4+} and Tb^{4+}) have strong charge-transfer bands, while the divalent rare earth ions (Eu^{2+}, Sm^{2+} and Yb^{2+}) have strong 4*f*-5*d* transitions. Trivalent rare earth ions that can be reduced have charge-transfer bands in the ultraviolet, and trivalent ions that can be oxidized have 4*f*-5*d* transitions in the ultraviolet. Thus, in general, the strong transitions do not give rise to physical coloration, but have a strong channel for excitation luminescence because of UV absorption, either by their own internal transitions, or by energy transfer to nearby activators. Both charge transfer and 4*f*-5*d* transitions produce broad absorption and emission peaks due to $\Delta R \neq 0$ (Fig. 14).

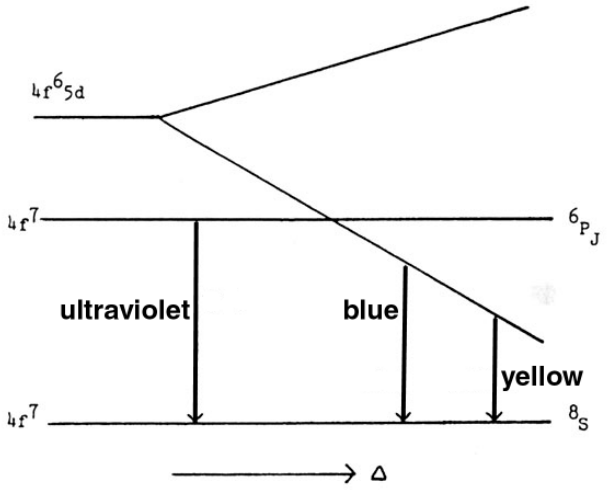

Figure 14. A simplified energy level diagram showing why there is significant difference in the line (band) widths for *f-f* vs. *d-f* transitions in Eu^{2+}. As the crystal field is increased (Δ) the spacing of the 4*f* states does not change due to their symmetry agreement. However, the 4*f*5*d* state drops appreciably in energy. For low crystal fields the *f-f* emission band will be quite narrow, while for high fields the $4f^6 5d$ to $4f^7$ transition will be very broad. See also Figures 1 and 7. Modified after Shionoya and Yen (1999).

f-d transitions: Eu^{2+}, Sm^{2+} and Yb^{2+}. Divalent Eu is an important activator in many minerals (Mariano and Ring 1975, Roeder et al. 1987, Gaft et al. 2001b), and is the activator responsible for fluorite's frequent strong blue luminescence, a phenomenon that first attracted Stokes' attention in studying fluorescence (Stokes 1852). Eu^{2+} emission is dependent on the local crystal field strength and symmetry, and thus apatite structural

COLOR PLATES

Color Plates 1-4: From Chapter 3, Rakovan (this volume).

Color Plate 1. Figure 15 in Rakovan, this volume, page 72. Fluorapatite from the Siglo XX Mine, Llallagua, Bolivia. (*left*) In plane light. (*right*) In long wave ultraviolet light. Photoluminescence is activated by REEs. Differential luminescence between {001} faces (violet) and {100} faces (orange), indicates sectoral zoning of REEs.

Color Plate 2. Figure 20 in Rakovan, this volume, page 75. (*left*) Cathodoluminescence (REE-activated) photomicrograph of the growth hillock in the right image. Luminescence (orange) is homogenous between the two symmetrically equivalent vicinal faces. Differential luminescence exists between these and the symmetrically nonequivalent vicinal face (blue). *right*) DIC photomicrograph of a trigonal growth hillock on the {100} face of a fluorapatite from the Golconda Mine, Minas Gerais, Brazil. [Used by permission of the Mineralogical Society of America, from Rakovan and Reeder (1994) American Mineralogist, Vol. 79, Fig. 6 p. 897].

Color Plate 3. Figure 21 in Rakovan, this volume, page 75. (*left*) DIC photomicrograph of a trigonal growth hillock on the {100} face of a fluorapatite from the Siglo XX Mine, Llallagua, Bolivia. Steps of [$0\bar{1}1$] orientation comprise vicinal face **a**, and steps of [001] orientation comprise vicinal face **b**. (*right*) Cathodoluminescence photomicrograph of the hillock in left image. Luminescence is homogenous between the two symmetrically equivalent vicinal faces (yellow luminescence activated by Mn^{2+}). Differential luminescence exists between these and the symmetrically nonequivalent vicinal face (blue activated by REEs). [Modified after Rakovan and Reeder (1996)].

Color Plate 4. Figure 24 in Rakovan, this volume, page 77. (*left*) Cathodoluminescence photomicrograph of hexagonal growth hillocks on the {001} face of an apatite from the Siglo XX Mine, Llallagua, Bolivia. Luminescence (purple activated by REEs) is homogenous among the six symmetrically equivalent pyramidal vicinal faces. Yellow luminescence (Mn^{2+}-activated) dominates flat regions of the {001} face and the terminal surfaces of the hillocks. (*right*) DIC photomicrograph showing the microtopography of the {001} apatite face in the left image. [Used by permission of the Mineralogical Society of America, from Rakovan and Reeder (1994) American Mineralogist, Vol. 79, Fig. 7, p. 897].

Color Plates 5-16: Figure 6 in Waychunas (this chapter).

Photoluminescence (short-wave ultraviolet, SWUV, Mid-wave ultraviolet, MWUV, and long-wave ultraviolet, LWUV) of apatites from various localities with postulated major luminescent centers, based on various unpublished data. Photos taken with Canon 4 Mb digital camera equipped with UV filter and close-up capability. Exposures 0.5-10 seconds. Colors adjusted with Photoshop 6.0 to agree with observed emission in a dark room.

~~~~~~

Color Plate 5. Fluorapatite, Cerro Grande Mine, La Paz, Bolivia. Sector zoned: blue {001} and {101} sectors and violet {100} sectors. Eu^{2+}/Ce^{3+}-activation. Largest crystal is 60 mm. SWUV.

Color Plate 6. Fluorapatite, Greenwood, Maine, USA. (pinkish-red) Eu^{3+}-activation. Matrix of luminescent albite (blue) activated by Eu^{2+}. Largest crystal is 10 mm. SWUV.
~~~~~~

Color Plate 7. Fluorapatite, Nuristan, Afghanistan. Mixed areas of REE- and Mn^{2+}-activation. Specimen is 100 mm across. SWUV.

Color Plate 8. Fluorapatite, Panasqueira, Portugal. Center (yellow) Mn^{2+}-activation; ends (blue) Eu^{2+}-activation. Zoning is probably due to a combination of temporal variations in solution chemistry and face-specific incorporation. Largest crystal is 25 mm. SWUV.

Color Plate 9. Fluorapatite associated with (or altering to) autunite. Ritchfield Pegmatite, Connecticut, USA. Mn^{2+} (yellow) and uranyl (green) activation. 100 mm sample. SWUV.

Color Plate 10. Johnbaumite, Jacobsberg, Sweden. Eu^{3+} and Sm^{3+} activation (pink-violet). Matrix is fluorescent calcite (red) activated by Mn^{2+} and Pb^{2+}. 60 mm sample. SWUV.

Color Plate 11. Fluorapatite, Imichil, Anti Atlas Mtns., Morocco, exhibiting concentric zoning. Eu^{2+} activation. 300 mm specimen. MWUV.

Color Plate 12. Fluorapatite, Franklin, New Jersey, USA. Mn^{2+}-activation (red). Other luminescent minerals: (green) willemite, activated by tetrahedral Mn^{2+}; (pink-red) calcite, activated by Mn^{2+} and Pb^{2+}; non-luminescent (black) franklinite. 200 mm specimen. SWUV.

Color Plate 13. Fluorapatite, Durango, Mexico. See Figure 4 in (this chapter, page 706) for luminescence spectra. Purple fluorescence activated by Ce^{3+}, Eu^{2+}, Sm^{3+} and Dy^{3+}. Green fluorescence is hyalite opal with uranyl-activation. 200 mm specimen. MWUV.

Color Plate 14. Hydroxylapatite, Molina Mine, Potosi, Bolivia. Concentric zoning with cores Mn^{2+}-activated; exterior Eu^{2+}-activated. 50 mm crystals. MWUV.

Color Plate 15. Fluorapatite from a granite pegmatite pocket, Gilgit-Skardu Road, Northern areas, Pakistan. Mn^{2+}-activation with bright yellow zones (Dy^{3+}?). Specimen exhibits strong yellow phosphorescence. 75 mm wide. SWUV.

Color Plate 16. Fluorapatite, Silver Crater Mine, Bancroft, Ontario (blue). Ce^{3+}- and Sm^{3+}-activation. Largest crystal is 150 mm. Fluorescent matrix (pink-red) is calcite activated by Mn^{2+}, Pb^{2+} and REE. MWUV.

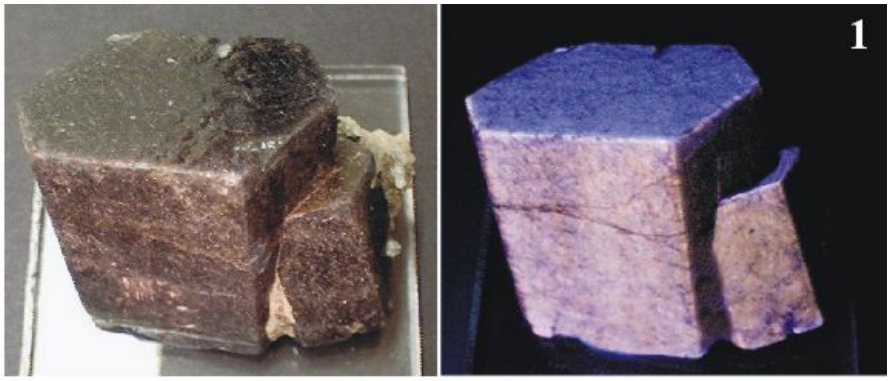
1

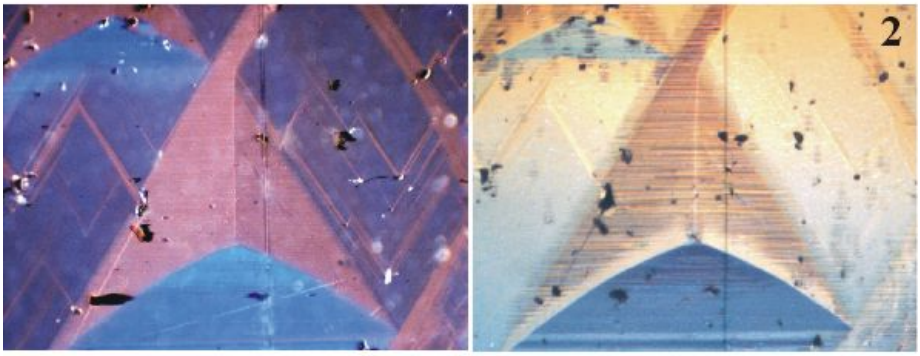
2

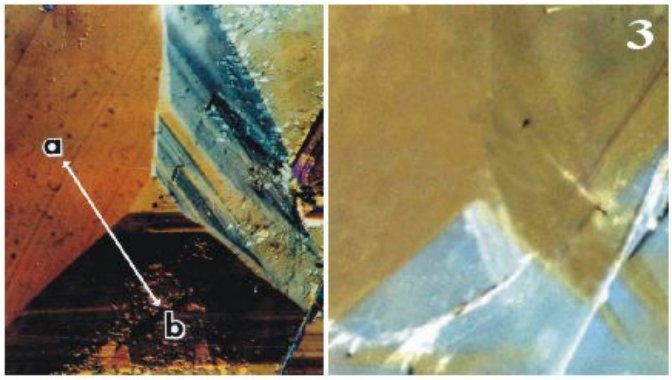
a
b
3

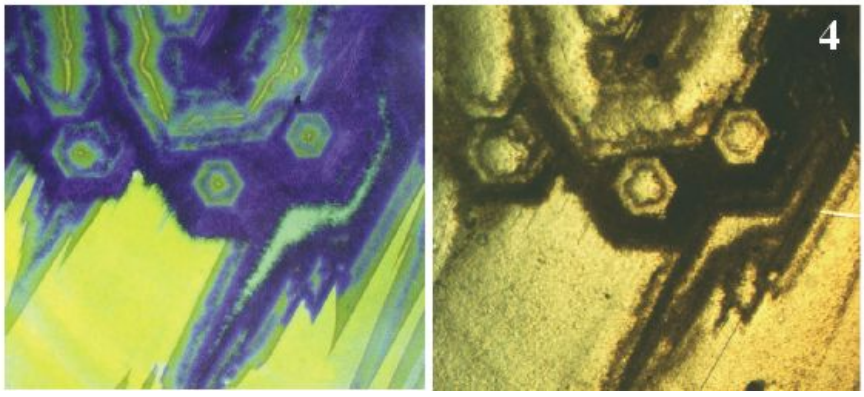
4

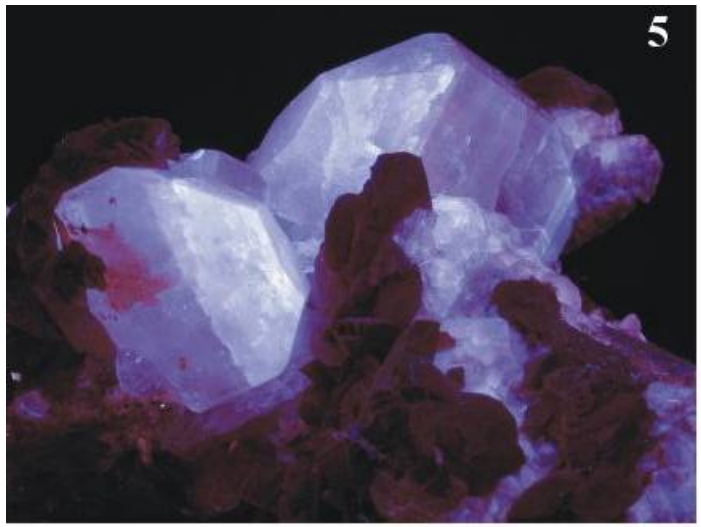
5


6


7


8

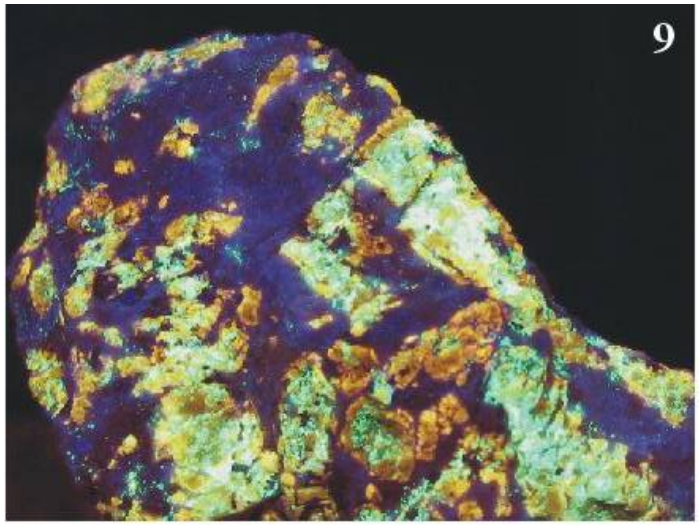
9

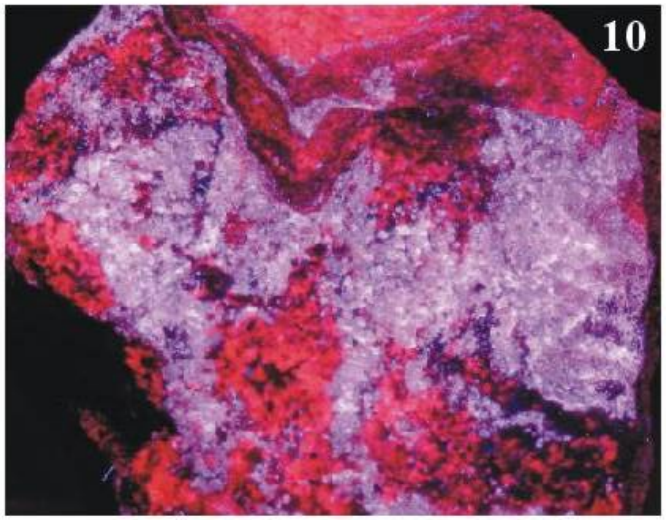
10

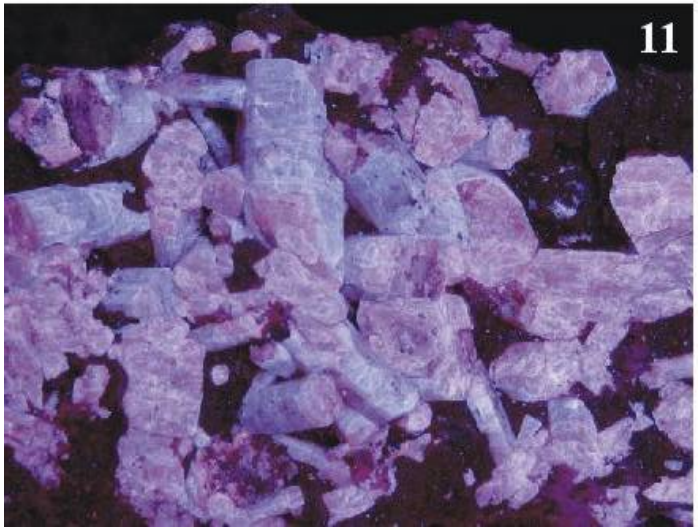
11

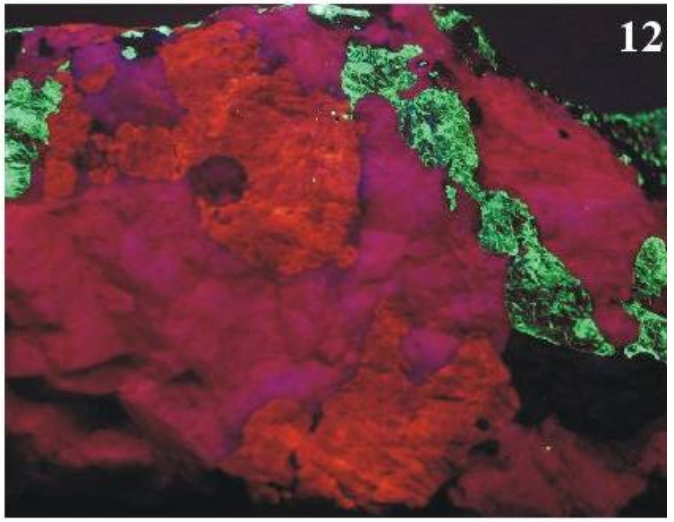
12

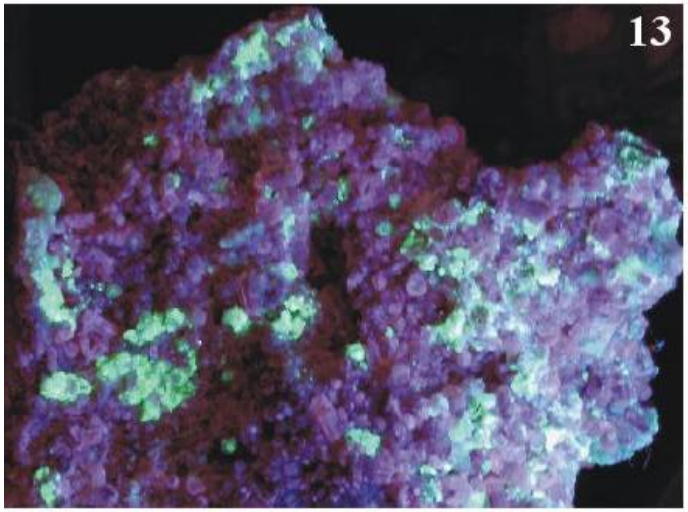
13


14


15


16

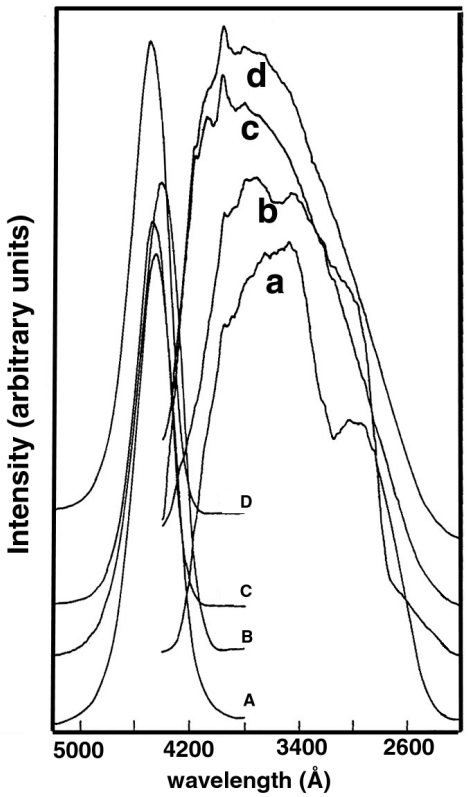

Figure 15. Shifts of both excitation (capital A-D) and emission bands (small a-d) in synthetic Sr apatites. (a) hydroxylapatite, (b) fluorapatite, (c) chlorapatite, (d) bromoapatite. Modified after Kottaisamy et al. (1994).

dimensions influence the luminescence spectrum. This effect is well shown in spectra collected by Kottaisamy et al. (1994) of doped synthetic apatites (Fig. 15) where Ca, Sr and Ba chlorapatites have Eu^{2+} emission bands at 450, 446 and 438 nm, respectively. In other minerals with 6-7 coordinated sites, Eu^{2+} emission can vary from 450 to 430 nm (Gaft et al. 2001b). CL spectra of apatites generally show Eu^{2+} bands at about 450 nm (Mitchell et al. 1997) although interference from Ce emission may overwhelm the Eu^{2+} signal. Gaft et al. (2001a) were able to separate the Eu^{2+} emission from a natural Ca-chlorapatite with considerable Ce and other rare earths using time-resolved spectroscopy (Fig. 16), also identifying a Eu^{2+} band at 450 nm. Other Eu^{2+} emission spectra have been reported by Jagannathan and Kutty (1997) and Gorobets (1981).

Eu^{2+}-Mn^{2+} energy transfer is an important process utilized in early halophosphate phosphors for fluorescent lamps. This is well known from excitation spectra of the Mn^{2+} emission, which show features of the Eu^{2+} absorption spectrum. In strontium chlorapatite doped with 2% Mn^{2+} and 2% Eu^{2+}, the Mn^{2+} emission increases in intensity and the Eu emission decreases in intensity with increase in temperature (Kottaisamy et al. 1994). This is due to increased transfer of energy from an excited Eu center to Mn^{2+} as temperature increases. Interestingly, the larger interatomic distances in barium chlor-apatite result in significantly reduced Mn^{2+} emission, probably due to reduced energy transfer. Energy transfer of this type has a very strong dependence on intersite distance (R), on the order of R^{-6} for electric dipole interactions, and R^{-8} for electric dipole/electric quadrupole interactions (Blasse and Grabmaier 1994). Hence small changes in lattice dimensions can produce dramatic effects in luminescence emission, where several types of energy transfer can occur, as with REE doped minerals. Thus energy transfer can bleed energy away from an excited Eu^{2+} so that Eu emission may vanish or be very weakened in response to lattice expansion, REE concentration levels, and type of REE impurity. This explains in part why CL and UV studies of Eu^{2+} in apatites, except in pure doped samples, are hard pressed to correlate Eu^{2+} composition and luminescent intensity.

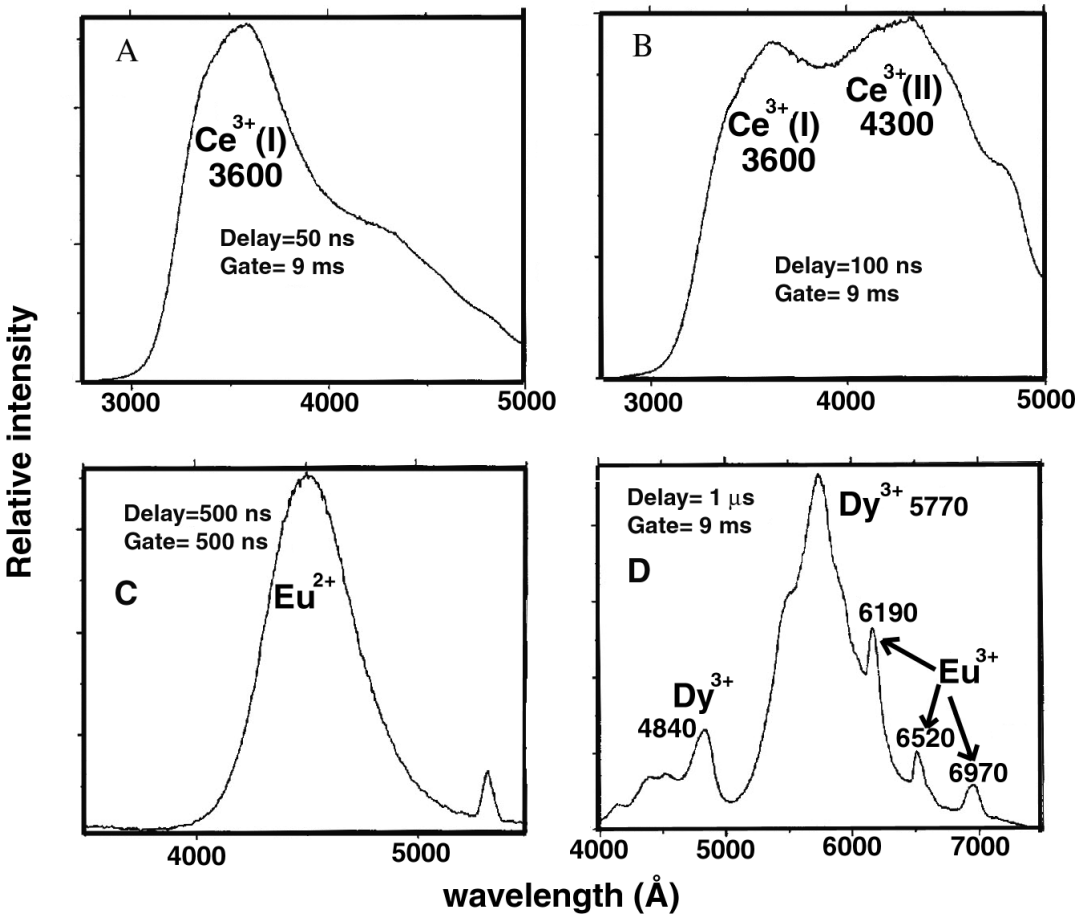

Figure 16. Time resolved laser-excited emission from green fluorapatite from Norway showing separation of REE emission due to lifetime differences. (a) Ce^{3+} emission with long gate and short delay. (b) slightly longer delay reveals both Ce centers. (c) shorter gate and longer delay separates out the Eu^{2+} emission. (d) longer delay and long gate show other REE emission. Modified after Gaft et al. (2001a).

In some cases, notably those with relatively short excited state lifetimes, energy transfer can be suppressed by excitation with laser pulses of shorter duration than the mean transfer time.

Sm^{2+} luminescence has been reported from natural anhydrite samples (Gaft et al. 1985, 2001a; Taraschan 1978) as a broad strong band at 630 nm. Other sharp bands are reported at 688, 700 and 734 nm. Sm^{2+} emission has not been reported for apatite, but the ion size and valence are amenable to the Ca sites, so ultimately it may be observed via pulsed laser techniques. $Sm^{2+}$is present in aqueous solution only under quite reducing conditions, so this may limit concentrations. Sm^{2+}does occur in fluorite, and is responsible for the strong green coloration and sensitized Eu^{2+} luminescence in that mineral (Robbins 1994). However, in fluorite the Sm^{2+} may be created by radiation effects which reduce bound Sm^{3+} ions. Yb^{2+} emission has not apparently been reported in any minerals, but has been studied in borates and oxides (Blasse and Grabmaier 1994). Its emission is in the UV at about the position of Eu^{2+} bands. Yb^{3+} emission is observed in apatite, hence Yb^{2+} might be created in naturally irradiated samples.

Trivalent rare earths. The trivalent rare earths may show 4*f*-5*d* or 4*f*-4*f* luminescence transitions. As with the divalent REE, the 4*f*-5*d* transitions will be broad, while the 4*f*-4*f* transitions will be sharp. Given the large number of possible states

(depending on the crystal field symmetry) there are many possible transitions. Thus given the many REE present in a given structure, a good chance exists that many of the transitions will be close in energy and thus favor energy transfer. Accordingly, not only can single energy transfers occur, but multiple ones involving several REE ions can occur as well.

Cerium. Cerium is the most common of the rare earths, and can have relatively high concentrations in apatites, e.g., Gaft et al. (2001a) lists a blue apatite containing over 4000 ppm Ce. Despite such high concentrations of Ce, specific Ce luminescence is infrequently observed, due to efficient energy transfer to manganese and other REE, and identification of the Ce^{3+} emission bands is rather ambiguous. CL spectra of Ce^{3+}-doped synthetic apatites show broad Ce^{3+} emission bands at 440 nm (0.18 % Ce, Mitchell et al. 1997), and 350, 380 and 458 nm (1% Ce, Blanc et al. 1995). CL emission from a natural fluorapatite from Portugal gave a single, very broad band at 349 nm (Knutson et al. 1985). Using UV excitation, Morozov et al. (1970) found two different bands at 395 and 420 nm in Ce^{3+} doped fluorapatite crystals. Shionoya and Yen (1999) list a range of emission wavelengths for Ce^{3+} in phosphors of 300-420 nm. In general, Ce^{3+} emission appears to be structure and even sample specific (Blasse and Bril 1967). However, Ce^{3+} emission can be identified unambiguously via absorption and excitation spectroscopy, or by time-resolved laser spectroscopy. Figures 16 and 17 show several Ce^{3+} fluorapatite emission spectra obtained from time resolved measurements (Gaft et al. 2001a) that suggest the Ce^{3+} emission band may differ depending on which Ca site is occupied. Gaft et al. (2001a) obtained band positions of 360 nm for Ce^{3+} in the Ca1 site, and 430 nm for Ce^{3+} in the Ca2 site in two different natural samples. Other minerals showed similar Ce^{3+} bands, notably zircon (355 nm), anhydrite (320 and 340 nm), barite (330 and 360 nm), danburnite (346 and 367 nm) and datolite (335 and 360 nm), with Ce^{3+} presumably substituting at a Ca site in all cases except zircon. In these samples, the Eu^{2+} emission bands were always at longer wavelengths, and thus distinctive. As the Ce^{3+} luminescence transition is from the lowest level of the 5*d* manifold to a spin-orbit coupling split 4*f*

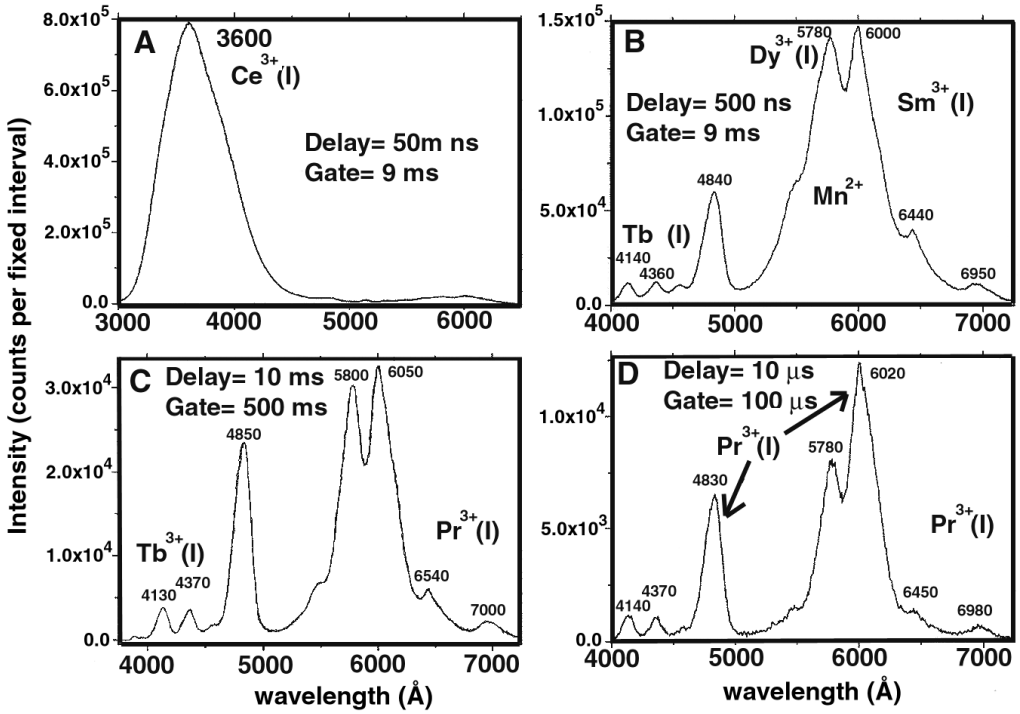

Figure 17. Emission from blue fluorapatite, Brazil, using a time resolved laser-excitation technique. Modified after Gaft et al. (2001a).

ground state, we expect two relatively broad bands for a given Ce^{3+} site (Blasse and Grabmaier 1994). Hence in all these minerals there are two bands for Ce^{3+} (except zircon), and in the Gaft et al. (2001a) apatite spectra the observed Ce^{3+} bands appear to each have two components that are incompletely resolved. In light of the result of Gaft et al. (2001a) the differing results of Mitchell et al. (1997) and Blanc et al. (1995) might conceivably be due to Ce^{3+} site partitioning as a function of dopant concentration.

Ce^{3+}-REE^{3+} energy transfer is strong for any REE ion that has transitions in the UV, such as Eu^{2+}, Pr^{3+}, Tm^{3+} and Tb^{3+}. Therefore in CL or photoluminescence spectra of apatites (and other minerals), Ce^{3+} emission may be quenched by energy transfer to these and other REE species, even with their concentration levels substantially lower than that of the Ce^{3+}. An example is given by the spectra of two fluorescent apatites from the Coldwell alkaline complex in Ontario (Mitchell et al. 1997). Both of these apatites have dominant Ce^{3+}, but only very weak emission in the general area of the Ce^{3+} bands. However, the Dy^{3+}, Sm^{3+} and Tb^{3+} emission bands are quite strong (Fig. 18). Contrariwise, Ce^{3+} emission might be expected to be strong in apatite group minerals with very low concentrations of other REE (and quenching ions), where the individual ions are too far apart on average for efficient energy transfer.

Praseodymium. Praseodymium is generally present at about 10% or less of the Ce^{3+} level in apatites. The CL spectrum of a synthetic doped sample shows two bands in the

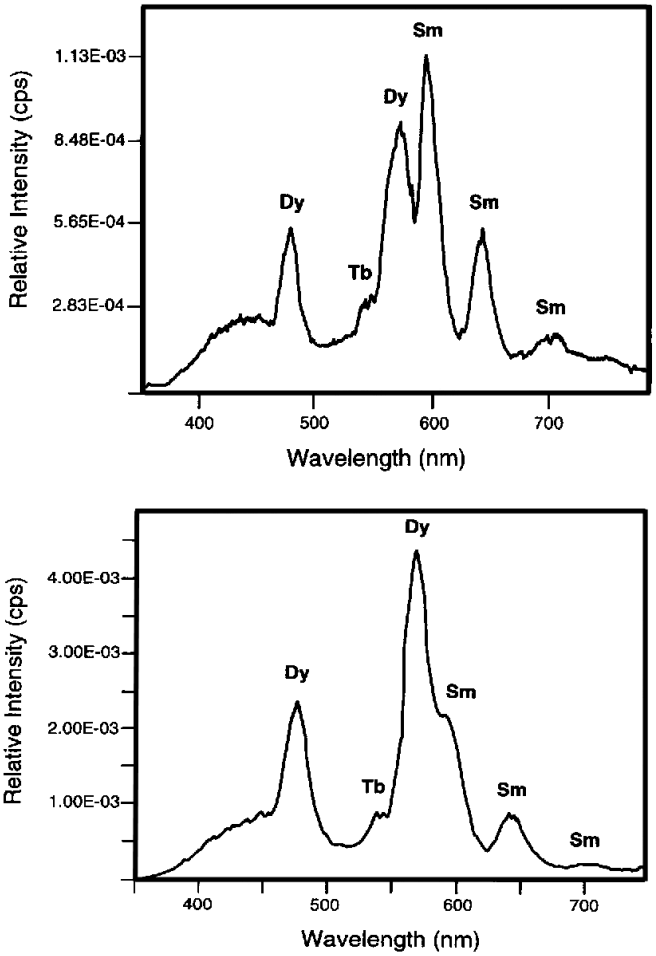

Figure 18. CL emission spectra of fluorapatite from the Coldwell complex, Ontario. Top: yellow-luminescent sample from a ferro-augite syenite in Center I. This type of emission may closely resemble Mn^{2+} broadband emission to the naked eye. Bottom: yellow-red luminescent sample from the same general region. Modified after Mitchell et al. (1997).

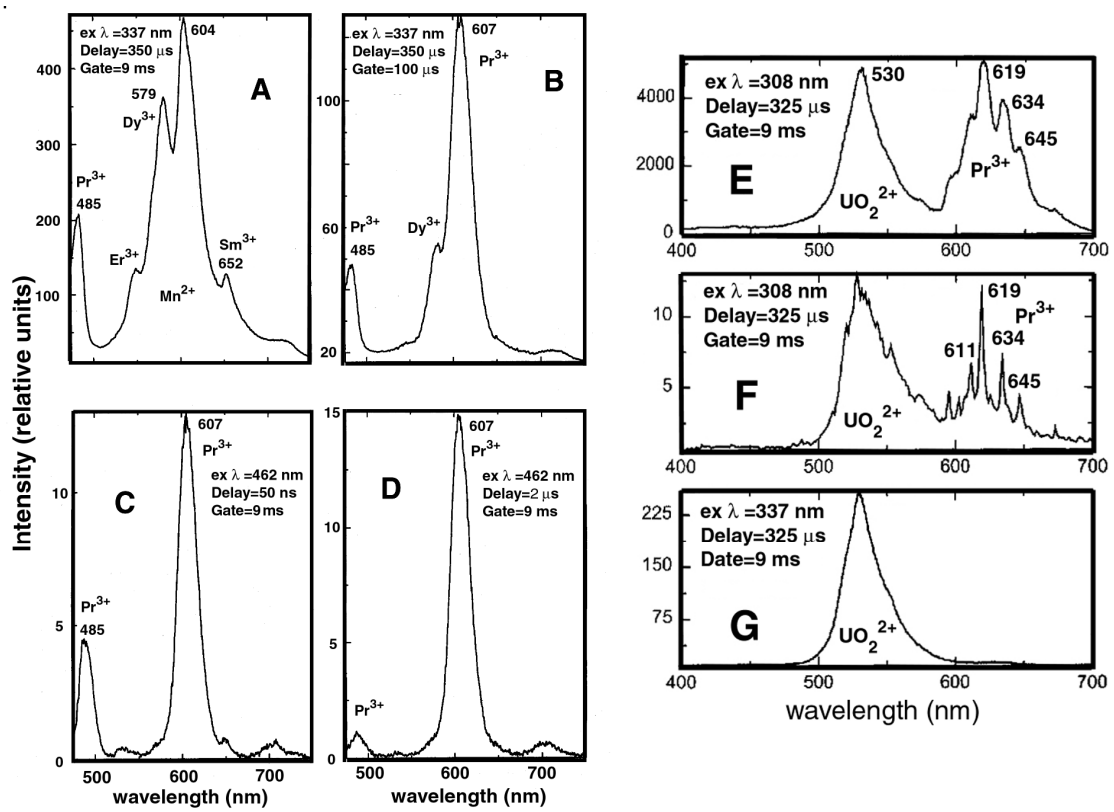

Figure 19. Pr^{3+} emission from a magmatic apatite revealed by time-resolved laser excitation. (A) and (B) 337 nm excitation. Shorter gate discriminates between Pr^{3+} and other REE emission. Delay stops quickly decaying Eu^{2+} and Ce^{3+} emission from obscuring the 485 nm band. (C) and (D) 462 nm excitation. Delay timing separation of Pr^{3+} emission. (E) Sedimentary apatite with uranyl and Pr^{3+} emission excited at 325 nm. (F) same as (E) but higher resolution spectral scan. (G) Pr^{3+} emission removed by excitation at 337 nm. Modified after Gaft et al. (1999).

UV at 248 and 278 nm, and sets of narrow bands centered at about 488 and 615 nm (Mitchell et al. 1997) yielding a brick-red emission color. Natural samples of hydroxyl-apatite and fluorapatite show similar CL bands (Gaft et al. 1999). Time-resolved emission spectra (Fig. 19) show well defined Pr^{3+} emission in natural magmatic apatite at 485 and 607 nm (Gaft et al. 1999). Studies using polarized emission measurements on this sample were interpreted as representative of only Ca1 site occupation by Pr^{3+} (Reisfeld et al. 1996). In contrast, a sedimentary apatite annealed in air showed a different Pr^{3+} spectrum, with a set of bands centered at about 630 nm (Fig. 19). This spectrum was interpreted to be due to Pr^{3+} in Ca2 (Reisfeld et al. 1996). Pr^{3+} appears to be an efficient sensitizer for Sm^{3+}, as many of its transition energies are almost identical to Sm^{3+}, and in general Pr^{3+} probably is more important as a sensitizer of other REE than for its own emission (Mitchell et al. 1997).

Neodymium. Neodymium can be present in relatively high concentrations in fluorapatites. Gaft et al. (2001a) lists Nd analyses for several natural apatites that are higher than any other REE except Ce, and at a concentration level of about 40% of the Ce value. Nd^{3+} emission is well into the IR, and it is not sensitized by most of the other REE. Hence, Nd^{3+} emission is expected to be relatively independent of other impurities, and will not contribute to visible luminescence. However, Nd^{3+}-doped synthetic apatites are excellent laser materials, due to several physical attributes of the Nd^{3+} electronic structure in the host lattice. Detailed evaluation of the optical properties of Nd^{3+} in Ba fluorapatite

are given by Stefanos et al. (2000). The laser applications are considered below.

Samarium. Samarium is an important REE for apatite luminescence as it is frequently present in significant concentrations, is usually an efficient emission site, can receive energy from many REE sensitizers, and can have a large effect on the visible emission colors. The *f-f* transition spectra of Sm^{3+} in synthetic doped apatite has been reported by Taraschan (1978), Morozov et al. (1970), Mitchell et al. (1997) and Blanc et al. (1995) with reasonable agreement. The emission spectrum consists of 4 large bands, each composed of many transitions, at 558, 594, 639 and 701 nm (Mitchell et al. 1997). These bands produce an emission color that is reddish-orange both via CL and UV excitation. Sm^{3+} emission in natural apatites (Fig. 20) is consistent with the bands observed in the synthetics (Mitchell et al. 1997, Murray and Oreskes 1997, Roeder et al. 1987, Barbarand and Pagel 2001). Laser-excited time-resolved emission spectra show Sm^{3+} bands at 600, 644 and 695 nm in a high-REE blue fluorapatite (Gaft et al. 2001a), and 567, 598 and 646 in a colorless fluorapatite (Gaft et al. 1998a). Splitting of the Sm^{3+} bands in a yellow fluorapatite emission spectrum was interpreted as being due to Sm^{3+} in Ca1 and Ca2 sites (Reisfeld et al. 1996) (Fig. 21)**.** Gruber et al. (1999) reported the absorption and emission spectra of Sm^{3+} in a synthetic Sr fluorapatite. The fluorescence intensities of the various bands were found to be similar to that for Sm^{3+} in doped glass laser material. These authors also have calculated the crystal field parameters for Sm^{3+} in the Ca2 site in Sr fluorapatite and the radiative lifetimes for the emission transitions.

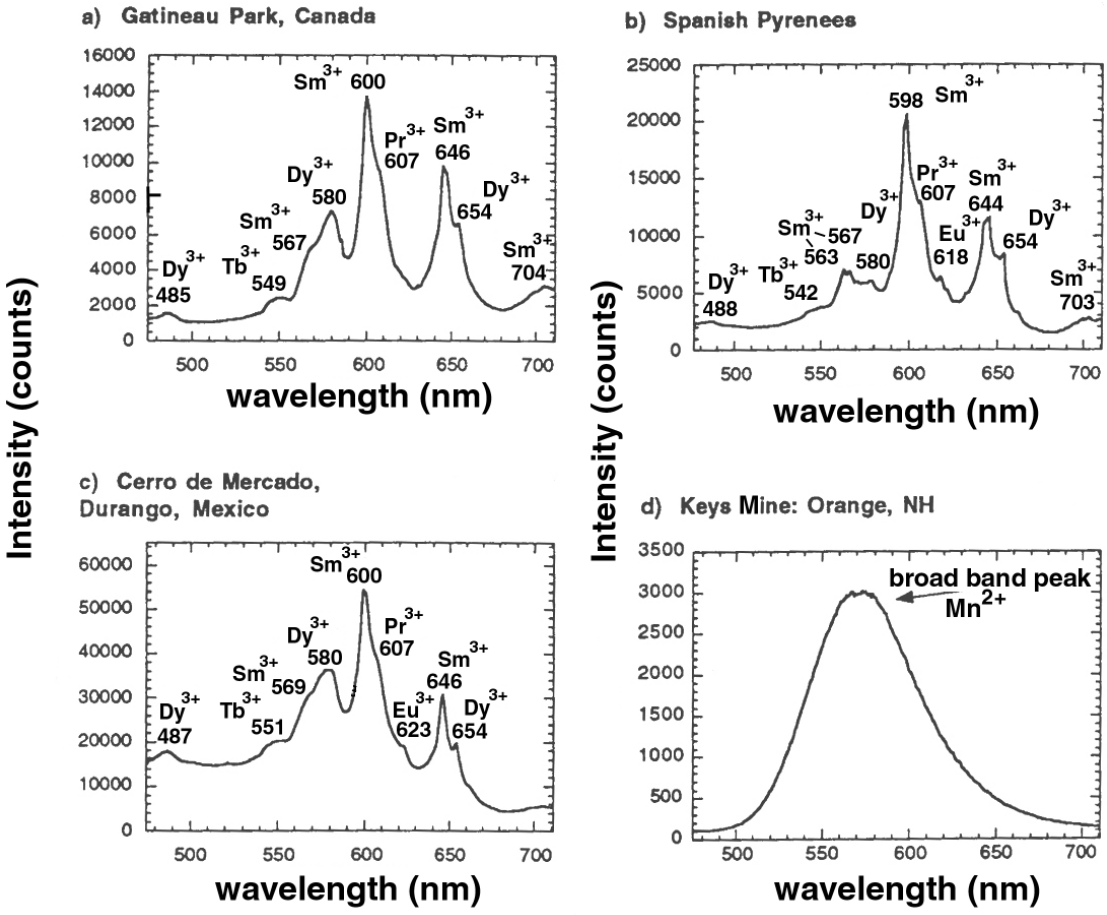

Figure 20. (a), (b) and (c) CL emission spectra for apatites with significant Sm^{3+} and other REE activators. Compare with the clean Mn^{2+} spectrum from the NH-apatite (d). Modified after Murray and Oreskes (1997).

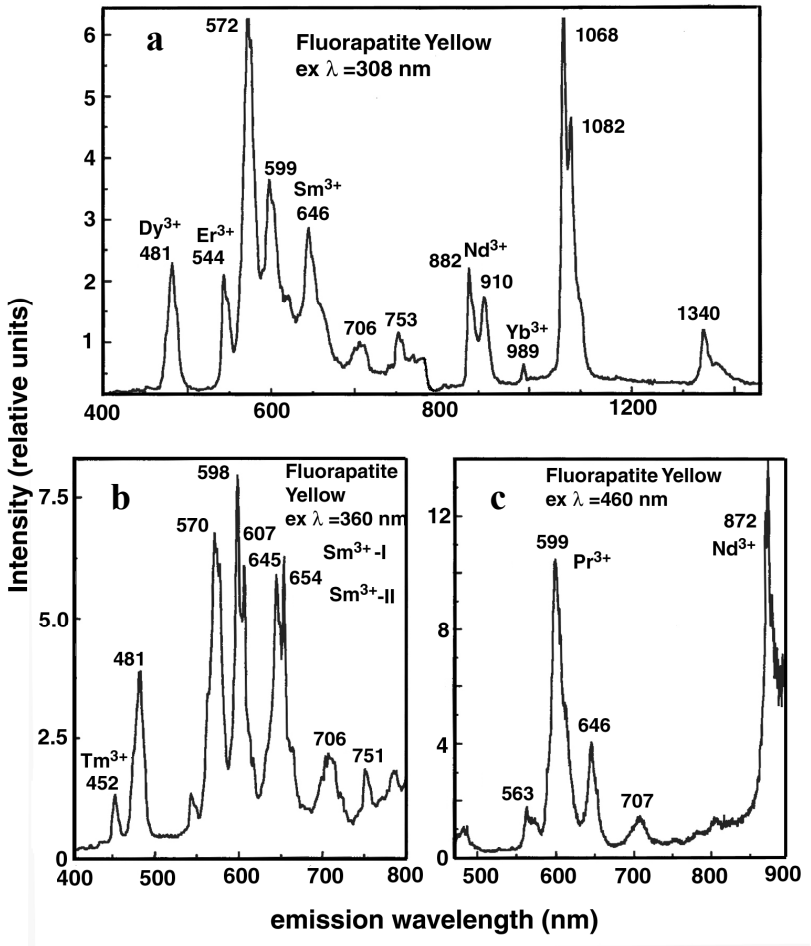

Figure 21. Laser excited fluorescence from a yellow fluorapatite. (a) Excitation at 308 nm. Note strong Nd^{3+} bands in the IR. (b) Sm^{3+} emission separated into contributions from Ca1 and Ca2 sites using 360 nm excitation. (c) Removal of Dy^{3+} emission using 460 nm excitation. Modified after Reisfeld et al. (1996).

Europium. Trivalent europium gives rise to red emission with CL bands at 587, 614, 645 and 694 nm (Mitchell et al. 1997, Mariano 1988, Mariano and Ring 1975, Roeder et al. 1987, Jagannathan and Kottaisamy 1995). All bands are due to *f-f* type transitions, and are composed of many such electronic transitions. As with other *f-f* emission spectra, doped synthetic apatite and natural apatite agree closely, but in natural samples there is considerable overlap of the 587 band with other REE emission features. Laser activated time-resolved spectra at 266 nm yield well defined bands at 579, 590, 618, 653 and 700 nm attributed to Eu^{3+} in the Ca1 site (Gaft et al. 1997a,b). Laser excitation at 337 and 355 nm allows detection of bands at 575, 628 and 712 nm that are attributed to Eu^{3+} in the Ca2 site because of shorter luminescence lifetime (Fig. 22). In general, a less symmetric site produces a shorter excited state lifetime by allowing increased lattice interactions. Eu^{3+} emission bands overlap with Sm^{3+} bands as well as bands from other REE. Hence assignment of Eu^{3+} features requires careful comparison with doped standards, and use of time-resolution measurement techniques if available. Piriou et al. (2001) obtained high resolution spectra of Eu^{3+} in a synthetic sodium lead apatite, and confirmed that Eu^{3+} spectra can be used to determine individual site occupations due to symmetry, splitting and lifetime effects. Eu^{3+} doped into synthetic Ca hydroxyapatite was also investigated by Ternane et al. (1999) with time-resolved techniques (see below).

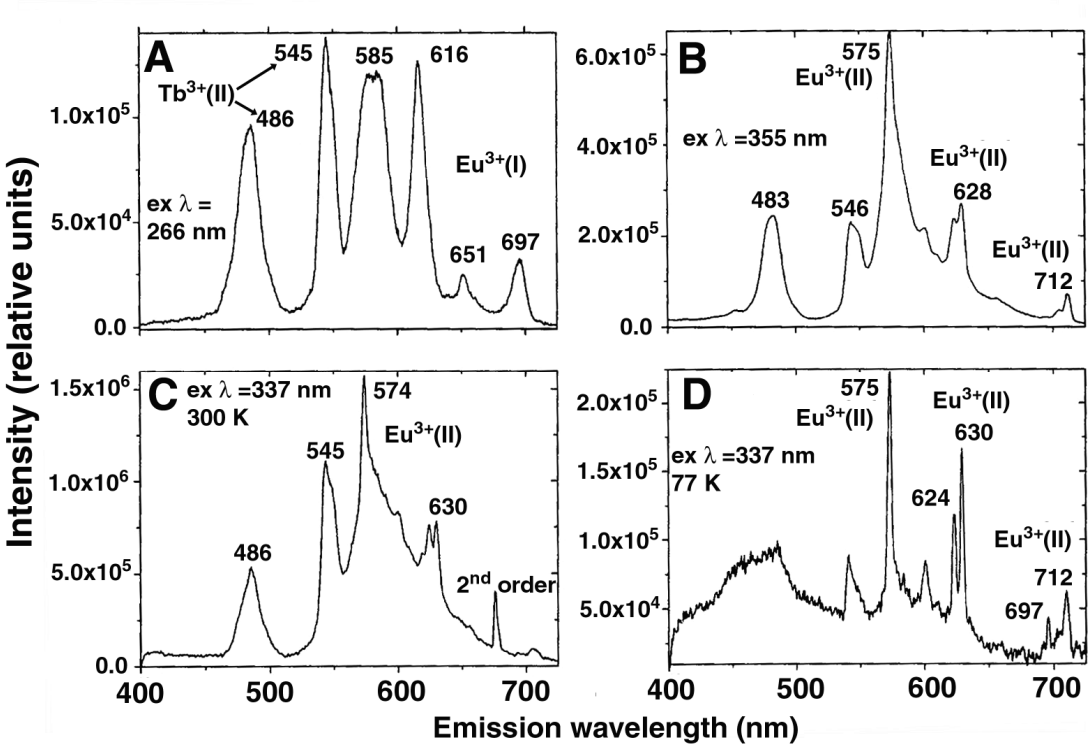

Figure 22. Comparison of strategies for separating emission bands using laser-excited luminescence on a Norway fluorapatite. (A-D) Effects of excitation wavelength and cooling.

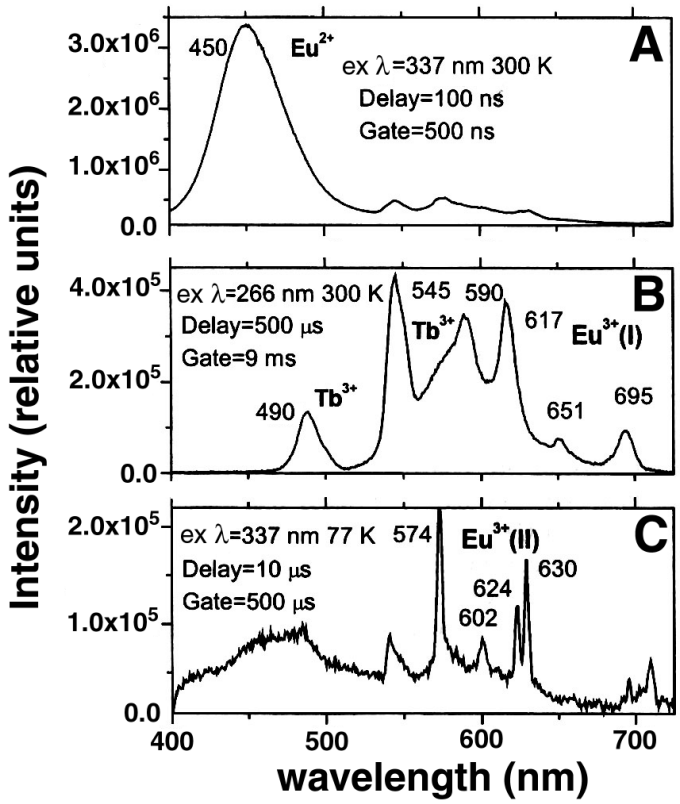

Figure 22, continued. Comparison of strategies for separating emission bands using laser-excited luminescence on a Norway fluorapatite.(A-C) Use of gate and delay timing to separate Eu^{2+} and multi-site Eu^{3+} emission bands. Modified after Gaft et al. (1997a,b; 2001a).

Gadolinium and terbium. Gd^{3+} *f-f* emission bands appear only in the mid-range UV (UVB), and do not contribute to visible luminescence. No spectra of Gd^{3+} in apatite or other Ca-containing minerals have been found in the literature. Terbium *f-f* emission spectra in synthetic fluorapatite have been measured by Blanc et al. (1995, 2000) via CL, and by Morozov et al. (1970) via photoluminescence with reasonable agreement. A large set of sharp bands is observed from 370 to 600 nm, with the main sets centered at about 375, 415, 490, 550 and 590 nm. The only band typically observed in natural apatites via CL or UV-excitation is at 545 nm (Roeder et al. 1987, Mitchell et al. 1997), and appears to have the longest lifetime of any of the emission states. Using laser-excitation and time-resolution Gaft et al. (2001a) found other Tb^{3+} bands at 380, 415 and 437 nm. These authors state that the 545 band is strongest in synthetic apatite and represents Tb^{3+} in the Ca2 site, while the 415 and 437 nm bands are due to Tb^{3+} in the Ca1 site and are strongest in natural apatites. This seems to be inconsistent with the other spectral observations for Tb^{3+} in natural apatite, including another spectrum reported by Gaft et al. (2001a) of a red natural apatite which shows only a strong 545 nm Tb^{3+} band (Fig. 22). Tb^{3+} can be a sensitizer for Eu^{3+} (Tachihante et al. 1996) so that its excited state energy may be resonantly siphoned off into excitation of Eu^{3+}.

Dysprosium. Dysprosium *f-f* emission bands produce a yellow luminescence. The CL emission spectrum in doped synthetic fluorapatite consists of bands at 475, 570, 657 and 746 nm, each composed of several sharp transitions visible in high resolution conditions (Mitchell et al. 1997). This spectrum agrees with CL and photoluminescence spectra collected by Blanc et al. (1995) and Morozov et al. (1970), respectively, also for synthetics. The Dy^{3+} bands in natural apatite group minerals are commonly observed, and often are some of the most intense REE contributions to the emission. We can infer from this that Dy^{3+} is probably the beneficiary of other REE acting as sensitizers. Mitchell et al. (1997) observed bands at 475 and 570 nm in all three of their natural apatite samples from the Coldwell alkaline complex. In another sample from Waldigee Hills, Australia with low REE content an unidentified band and another due to Mn could easily be reassigned to Dy^{3+}. Roeder et al. (1987) and Mariano (1988) observed similar bands in natural apatites from many additional areas. Barbarand and Pagel (2001) also detected a Dy^{3+} band at 665 nm in apatite from Arendal, Bamble, Norway. Laser excitation studies by Gaft et al. (2001a) in natural apatites reveals bands at the same positions, plus an additional band at 750 nm.

Holmium, erbium, thulium and ytterbium. Holmium appears to be a weak emission center compared to other divalent and trivalent REE, and will not contribute detectably to natural apatite emission spectra in the presence of Eu, Sm or Dy. A synthetic apatite CL spectra for Ho^{3+} has been collected by Blanc et al. (1995), and Gruber et al. (1997b) have investigated the emission spectrum in Sr fluorapatite. Holmium is a potential luminescence quencher due to non-radiative resonant energy transfer. Erbium, like Holmium, is a weak emission center, and not an important player in natural apatite luminescence. It has been explored as a dopant in Sr fluorapatite for use in laser applications (Gruber et al. 1997a). Er^{3+} spectra obtained from synthetic fluorapatite do not show agreement. The CL spectrum of a synthetic Er^{3+} apatite studied by Mitchell et al. (1997) shows only a broad band near 440 nm, resembling an Eu^{2+} band. In contrast, Blanc et al. (1995) obtained a CL spectrum with well defined bands at 319, 402, 471, 527 and 552 nm on a broad background. Although Er^{3+} bands are not assigned in any of their natural apatite emission spectra, several bands were observed in scheelite at 524 and 551 by Gaft et al. (2001a). Thulium is a weak luminescence activator (Mitchell et al. 1997) and not a significant contributor to apatite luminescence. A Tm^{3+} band has been observed by Gaft et al. (1998a) in a yellow fluorapatite from the Kola peninsula at 452 nm. This is in agreement with bands observed at 356 and 461 nm in synthetic doped fluorapatite

using CL by Blanc et al. (1995). Reisfeld et al. (1996) and Gaft et al. (1997b) associate the Tm^{3+} emission with Ca2 occupation. Gruber et al. (1998) have obtained the crystal field parameters for Tm^{3+} in the Ca2 site from optical spectra and lattice-sum electrostatic calculations. Ytterbium has no luminescence emission in the visible, with bands near 1000 nm (DeLoach et al. 1994). It is not important as a sensitizer or activator in natural apatites. Reisfeld et al. (1996) assigns the emission bands as due to Yb^{3+} occupation of the Ca2 site. Gruber et al. (1998) have derived the crystal field parameters for Yb^{3+} in the Ca2 site in Sr fluorapatite. Ytterbium can be sensitized by other REE ions, an example of this is shown in a cartoon from Marfunin (1979) in Figure 23.

Uranium. Hexavalent uranium as the uranyl group, UO_2^{2+}, and the uranate ion U^{6}+, have characteristic luminescence spectra in model compounds (Blasse et al. 1979, Blasse 1988, Blasse and Grabmaier 1994, DeNeufville et al. 1981). The linear uranyl ion yields characteristic vibronic emission spectral structure that is readily identified at low temperatures and is quite distinct from uranate ion spectra. Uranyl ion is known to substitute in many mineral structures, sometimes on lattice sites, and sometimes as an interstitial or inclusional impurity. In synthetic powder fluorapatites, recent EXAFS analysis by Rakovan et al. (2002) showed that hexavalent uranium (2.6 wt %) was present mainly as the uranate species, with six approximately equal U-O distances of 2.06 Å. The uranate resided mainly in the Ca1 site and utilized the innermost six oxygen ligands. Luminescence spectra was consistent with this assignment. This result is interesting as most hexavalent uranium in mineral structures and in aqueous solutions is believed present as the uranyl specie. For example, Gaft et al. (1996b, 1999) examined fossil apatites (see below) and concluded that the uranium content was diagenetic in origin and only included uranyl ions. In sedimentary apatite Panczer et al. (1998) determined that uranyl was present both as sorbed complexes, and as films of uranyl-bearing minerals, based on both emission spectra and lifetime measurements. However, in magmatic apatites Panczer et al. (1998) did not observe uranium luminescence until after a 1100 K anneal. This led to the suggestion that the uranium was originally present in the tetravalent state. This is indeed permissible due to its similar ionic radius (0.97 Å) compared to Ca (0.99Å). Such a substitution could be charge balanced by Na substitution for Ca in two Ca sites. It was further conjectured that during the anneal uranium was oxidized to the hexavalent state, and formed a complex with OH and F ligands from the apatite.

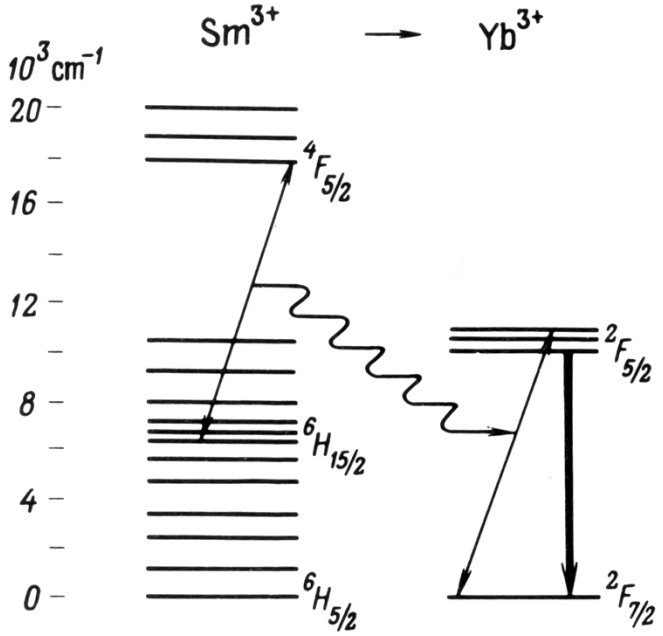

Figure 23. A possible mechanism for energy transfer from Sm^{3+} to Yb^{3+}. This type of transition is common among trivalent REE due to similar state symmetry and transition energies. The heavy line in the Yb^{3+} state diagram is the ultimate emission transition. Modified after Marfunin (1979).

Luminescence in other apatite group minerals

Hydroxylapatite $Ca_5(PO_4)_3(OH)$, carbonate apatites and biological apatite have been extensively examined due to their significance in human and animal skeletal and dental material (Elliott 1994, McConnel 1973, Grandjean-Lecuyer et al. 1993, Gotze et al. 2001). However, CL and other fluorescence emission have been less studied, in part due to the usually very low concentrations of Mn^{2+} (about 1 ppm) and REE activators (often well below 1 ppm) in the biological samples, and the inapplicability of hydroxylapatite and carbonate apatites for phosphor utilization. Habermann et al. (2000) studied apatite samples and fossil conodonts (francolite-carbonate apatite) with micro-PIXE, CL and ESR. They found that the concentration distribution of REE in the conodonts were inconsistent with REE concentrations in seawater, and also different from that in recent fish bone debris. In particular, Ce^{3+} and Eu^{3+} were enriched relative to both standards. They concluded that most of the REE were added during diagenetic alteration. CL spectra showed variations in REE composition with position in the conodonts, and strong contributions from trivalent Sm, Dy, and Tb (Fig. 24). Habermann et al. (2000) also refer to an "intrinsic" blue emission from the conodonts, which is not explained. Gaft et al. (1996a,b) examined the laser-excited emission from fossil fish teeth from phosphorite deposits in Israel. Untreated samples showed bands due to uranyl ion with a short lifetime and possible organic material with very long lifetimes, always occurring together in the

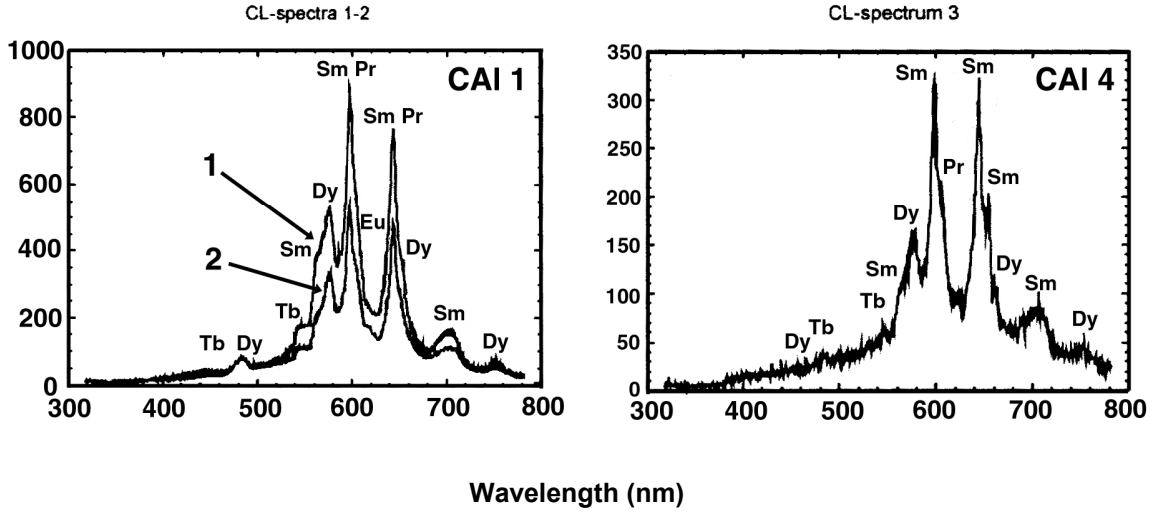

Figure 24. Cathodoluminescence spectra of Triassic conodonts (carbonate-fluorapatite) from Germany. 1 and 2 in the left-hand spectra refer to two points on the same fossil. Modified after Habermann et al. (2000).

same relative intensity, suggesting a mixture of uranyl with organic contaminants (Fig. 25). Annealing of the samples at 1000 K produced a better resolved and more intense uranyl emission, a reduced organic emission, and appearance of REE bands from several species. The authors speculated that dehydration and organic loss may have removed quenching mechanisms from the REE environments, e.g., coordination with water molecules. In work on synthetic hydroxylapatites, Ramesh and Jagannathan (2000) examined colloidally-formed nanocrystals of Sr chlorohydroxylapatite with Ce^{3+} dopant. They found that the luminescence was complex and markedly affected by changes in preparation conditions, possibly due to varying ratios of structural, surface and intergrain sites for the activator. Luminescence studies of Eu^{3+} in synthetic precipitated Ca hydroxylapatite (Ternane et al. 1999) showed less complexity, and a preference for the Ca2 site with two types of charge compensating neighbor arrangements.

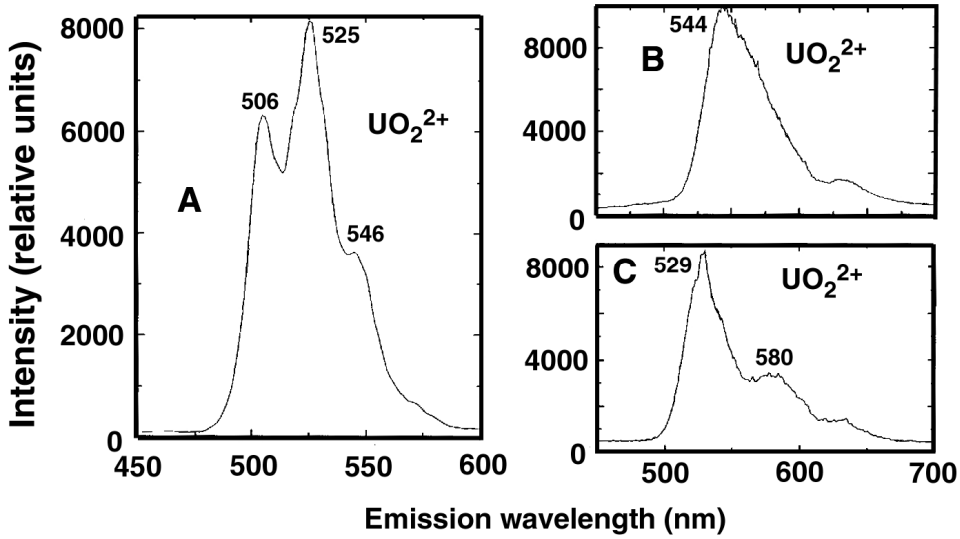

Figure 25. Laser-excited luminescence in fossil fish teeth from phosphorite beds in the Senonian Mishash formation, Israel. (A) Uranyl emission at 77 K indicating uranyl aqueous complexes. (B) after annealing at 1000 K the uranyl complexes are "dehydrated". (C) Same as in A but spectrum collected at 300 K. From these data it was concluded that the uranyl resides in organic material and not in the apatite structure. Modified after Gaft et al. (1996b).

Arsenate apatites Johnbaumite $Ca_5(AsO_4)_3(OH)$ and Svabite $Ca_5(AsO_4)_3F$ are noted above as having luminescence somewhat contradicting other observations. Some of the inconsistencies may be due to improper identification of samples characterized by UV light excitation. Svabite from Långban, Sweden has strong orange emission in samples studied by the author, but can be intimately admixed with other apatite group minerals with slightly different fluorescence. Svabite from Franklin, New Jersey has similar luminescence, perhaps slightly shifted to more yellow color. Johnbaumite from Jacobsberg, Sweden has interesting pink-violet UV-excited fluorescence that slightly varies over a specimen. It commonly occurs admixed with luminescent svabite and calcite, yielding samples with three color emission: deep red, orange, and pink-violet. Johnbaumite from Franklin, New Jersey, in contrast, seems to always show the orange emission. This suggests that the Jacobsberg samples have considerable REE activation (probably Eu^{2+} or Ce^{3+}), while the Franklin samples have mainly Mn^{2+} activation.

Lead arsenate apatites hedyphane $Pb_3Ca_2(AsO_4)_3Cl$, and mimetite $Pb_5(AsO_4)_3Cl$ are often luminescent, and the author has verified yellow-orange UV-excited emission in mimetite from Långban. Some of the mimetite samples have a golden emission that is particularly beautiful in association with luminescent calcite and svabite. Mimetite from Johanngeorgenstadt, Saxony, Germany show a yellow-orange emission under SWUV, but a pink emission under LWUV (Robbins 1994). This type of emission color change is not unusual in apatite group minerals. It is likely due to mainly Mn^{2+} emission from SWUV excitation, and combined Mn^{2+}, Ce^{3+}, and Eu^{2+} emission from LWUV excitation. As Pb^{2+} absorption is strong for SWUV but not LWUV, SWUV will excite $Pb^{2+} \rightarrow Mn^{2+}$ energy transfer and strong Mn^{2+} emission.

Lead apatites pyromorphite $Pb_5(PO_4)_3Cl$ and turneaurite $Pb_5(AsO_4,PO_4)_3Cl$ are also commonly fluorescent. Turneaurites from Franklin, New Jersey and Balmat, New York have an orange and orange-red emission, respectively, under UV excitation. Pyromorphite generally has strong physical coloration, which filters luminescence, but orange to yellow UV-excited luminescence has been observed in specimens from Broken Hill, NSW, Australia (Gait and Back 1992). Robbins (1994) mentions pyromorphite from

Granite Co., Montana that has a strong orange emission under LWUV, and pink-orange luminescence has also been observed in samples from several localities.

Vanadinite $Pb_5(VO_4)_3Cl$ is generally a strongly colored mineral that rarely shows fluorescence, but the weakest colored varieties, straw-yellow in physical color, can show yellow or greenish-yellow emission. Robbins (1994) notes that such vanadinite from Santa Eulalia, Chihuahua, Mexico is probably endlichite, with a large amount of arsenate substituting for vanadate.

LUMINESCENCE ZONING

Study of luminescence zoning can yield a wealth of information about the morphologic history of a crystal, changes in the environment during crystal growth, growth mechanism, structural differences at the crystal surface, and single crystal ages (Rakovan and Reeder 1994, 1996; Shore and Fowler 1996, Coulson and Chambers 1996, Rakovan et al. 1997, Rakovan et al. 2001). The most familiar type of luminescent zoning observed in apatite is concentric zoning; luminescent differences between concentric layers from the center of the crystal outward. Concentric zoning reflects temporal changes in the environment while a crystal is growing. Figure 6—Color Plates 11 and 14—show concentric zoning. The luminescence zoning seen in Figure 6—Color Plate 8—reflects a type of concentric zoning (temporal variation in luminescent activators) where the last stages of growth occurred at the ends of the crystals only. Oscillatory zoning, similar in appearance to concentric zoning, is thought in many cases to be due to quasiperiodic fluctuations in the chemistry at the mineral-solution or mineral-melt interface caused by diffusion-limited supply of growth units or substituent ions to the crystal surface (Shore and Fowler 1996). Oscillatory zoning is usually distinguished from normal concentric zoning by the scale of the zonation pattern, from tens of nanometers to tens of microns. Selective attachment and incorporation of substituent elements between structurally different regions of apatite surfaces give rise to two similar types of luminescent zoning, sectoral and intrasectoral zoning (Rakovan this volume). Sectoral and intrasectoral zoning of Eu^{2+}, Ce^{3+}, Eu^{3+}, Sm^{3+} as well as Mn^{2+} leads to spectacular cathodoluminescence zoning in apatites from Llallagua, Bolivia and the Golconda Mine, Minas Gerais, Brazil (see Color Plates 1-4; Figs. 15, 20, 21, 24-26 in Rakovan, this volume, p 51ff).

APATITE THERMOLUMINESCENCE

Thermoluminescence (TL) is a widely used technique for the determination of shallow energy states in solids due to trapped electrons and holes. The basic principle is that an applied temperature will release trapped electrons when kT (k = Boltzmann constant, and T = absolute temperature) is equivalent to the energy difference between the trapped state and the conduction band. Hence a type of spectrum is produced by slowly ramping the temperature of a material while its spectral emission is detected. Such a spectrum is called a glow curve, and usually plots all emitted photon intensity without discrimination of wavelength. After such a spectrum has been obtained, the full emission spectrum for every peak (i.e., temperature) in the glow curve can be obtained. In this way the ions associated with each trapping state can be identified (McKeever 1985).

TL is used for determination of equilibration temperatures in minerals, i.e., the highest temperature the mineral has experienced with sufficient time to empty traps corresponding to that or lower energies. In this case the threshold for the appearance of any emission is roughly equivalent to the equilibration temperature. Another use of TL is in dating materials and artifacts. In this case one must know the rate at which trapped electrons are generated in the material. As the electrons are normally trapped by the

action of high energy radiation, the integrated radiation dose may potentially be estimated from the measured TL emission, and then the age of the material calculated. This technique is widely used in determination of the age of pottery after firing, and is as accurate as the estimation of the dose rate allows.

TL is used in meteorite geochemistry to determine thermal history, terrestrial age, petrologic type, cosmic ray exposure rate, and other characteristics of meteorites (Sears 1980, Guimon et al. 1984, McKeever and Sears 1979). Remarkably, information on the orbital evolution of selected meteorites can also be determined using TL (Benoit and Sears 1997, 1991). As apatite can occur in practically every type of rock type, one might think that TL studies of apatites could be of significant use in terrestrial paleothermometry, but TL work has been limited. Ratnam et al. (1980) found that TL of a Mn^{2+} doped synthetic fluorapatite irradiated by x-rays from a laboratory source yielded glow curves with emission peaks at temperatures of 145, 185, 260 and 395°C. Spectra collected at several of these peaks showed the broad Mn^{2+} emission band. The band appeared to have two components at 560 and 595 nm, which were attributed to Mn^{2+} in the two Ca sites. Lapraz and Baumer (1983) collected TL spectra from thirty natural and five synthetic fluorapatites at temperatures between 77 and 750 K, both without treatment, and after x-ray irradiation. They found a large number of TL glow curve peaks, most of which could be associated with Mn^{2+} , Ce^{3+} , Eu^{2+} and Eu^{3+}. Individual spectra taken at the glow curve peaks showed good agreement with luminescence spectra in the literature (Figs. 26 and 27). Emission from other REE, though know to occur in the natural samples, was not observed. This suggests that those REE are not associated with trapping sites. An interesting result of this study and subsequent ones (Baumer et al. 1987, Lapraz et al. 1985) was the identification of a "lattice emission" band at about 400 nm which was believed to be associated with defects at the phosphate site. Perhaps this is the band identified by Habermann et al. (2000) as intrinsic in conodont emission spectra. This band was found to be strongest in undoped synthetic materials, and was quenched with addition of activators to synthetics or in natural samples, presumably due to energy transfer to the activator sites. Another finding was that many of the TL glow curve peaks were present even in the absence of activators, and were intensified with doping, or in naturals. This suggested that the peaks are related to intrinsic lattice defects, rather than to defect states associated with the activators. Results on hydroxyapatites and chlorapatites followed those from fluorapatite.

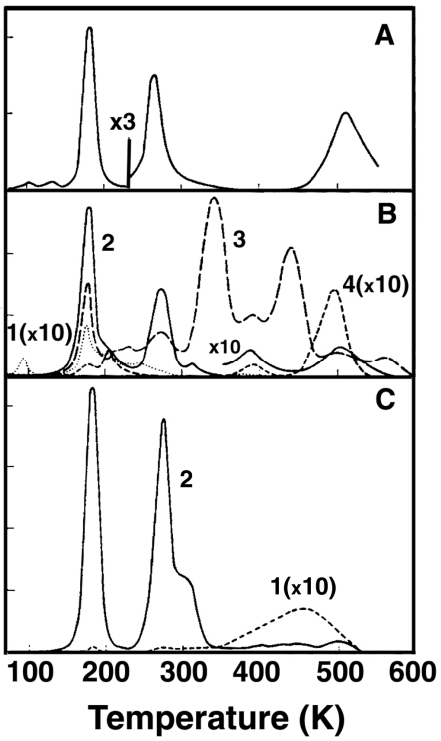

Figure 26. Thermoluminescent glow curves from synthetic fluorapatite after being irradiated with x-rays at 77 K: (A) doped with 0.2% Mn. (B) 1-undoped; 2-doped with 0.2% Mn; 3-doped with 0.2% Ce; 4-doped with 0.2% Eu. (C) 1- doped with 0.3% Mn; 2-doped with 0.3% Mn with hydrothermal anneal at 973 K. Each peak represents the emptying of a different set of trapped electrons. Modified after Lapraz and Baumer (1983).

A comparison of TL intensity with fission track density was done by Al-Khalifa et al. (1988) in a set of natural apatites. They found that increased densities of fission tracks were correlated with a decrease in TL sensitivity, or TL output per unit dose. The results

with the naturals were supplemented with apatite samples subjected to varying doses of 30 MeV alpha particles from a cyclotron, which verified the TL sensitivity reduction. Chlorapatites were more prone to the TL sensitivity loss than fluorapatites. This work indicates that apatites may be difficult to employ as radiation flux detectors, and thus not practical for long-term age dating.

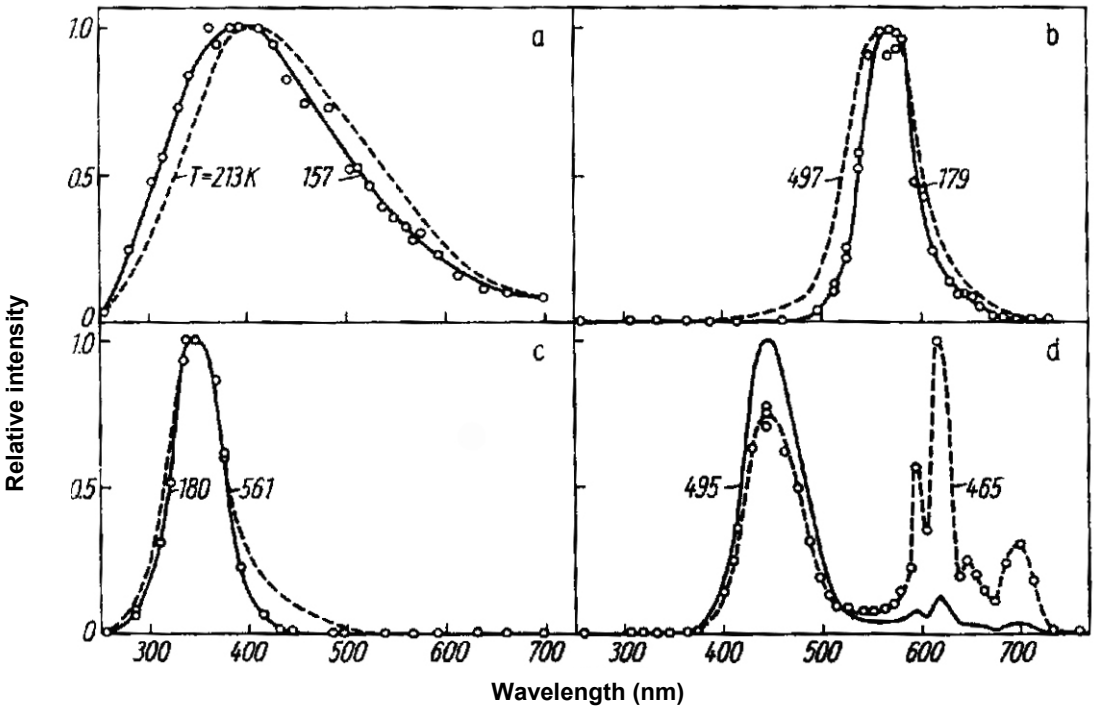

Figure 27. Synthetic fluorapatite emission spectra collected at glow curve maxima from Figure 26. (a) undoped. (b) 0.2% Mn. (c) 0.2% Ce. (d) 0.2% Eu. Modified after Lapraz and Baumer (1983).

SYNTHETIC APATITE USE IN FLUORESCENT LAMPS AND LASERS

Fluorescent lamp phosphors

Early fluorescent lamps (1938-1948) utilized mixtures of two phosphors, $MgWO_4$ (scheelite structure with broad band emission at 480 nm) and $(Zn,Be)_2SiO_4:Mn^{2+}$ (phenacite structure with two broad bands at 525 and 600 nm). These phosphors were initially replaced due to the poor lifetime of the phenacite phosphor, but the toxic aspects of the Be was also a consideration. Chloro- and fluor-apatites (called halophosphors) have been used since 1948 (Blasse and Grabmaier 1994, Jenkins et al. 1949). Numerous different activators and coactivators have been tested in apatite host matrices, but few have been found to be practical. For example, Ce^{3+} doped fluorapatite, either alone or coactivated with Mn^{2+}, develops parasitic emission bands that markedly affect emission color (Chenot et al. 1981). However, Eu^{2+}, Sb^{3+} and Mn^{2+}-Sb^{3+} doped halophosphors are efficient and resist degradation. Remarkably, the precise site occupation of the Sb^{3+} remains in question. Oomen et al. (1988) were able to explain the luminescence spectra and optical properties of Sb^{3+} by assuming a strong Jahn-Teller effect on the excited state. Their analysis was consistent with Sb^{3+} occupation of a Ca site. The structure of Sb^{3+} doped calcium fluorapatite was investigated by DeBoer et al. (1991) via Rietveld powder x-ray diffraction. They found that most of the Sb^{3+} appeared to enter the Ca2 site in a 2.2 wt % antimony sample (0.185 Sb atoms per 10 Ca atoms). However, a 3.1 wt % antimony sample gave conflicting results, indicating defect site occupation. In contrast, Moran et al. (1992) examined a series of Ca fluorapatites doped with 0-3.0 wt% Sb^{3+} via

^{19}F and ^{31}P magic-angle spinning NMR. They found evidence for Sb^{3+} occupation of the phosphate site. Table 1 (information from Shionoya and Yen 1999) shows a list of lamp phosphors in common use. Representative emission spectra are shown in Figure 28.

A white halophosphor has one major drawback, as it cannot be optimized for both high brightness and high color rendering. Color rendering refers to the ability of a light source to accurately match the output of a black body source with respect to color perception. If the rendering is poor, objects do not appear to the naked eye as having realistic colors and the color rendering index, or CRI, will be low. Blasse and Grabmaier (1994) note that at highest brightness for a white halophosphor (80 lumens/Watt), the CRI is about 60, while if the Mn and Sb levels are adjusted to obtain a CRI of 90, then the brightness drops to about 50 lumens/Watt. Using three phosphors (two activated by REE) solved this problem. The resulting "three color lamp" has phosphors with relatively narrow emission bands at 450, 550 and 610 nm. It can reach an output of 100 lumens/Watt while having a CRI of 85. Usually only the blue phosphor of this set is a

Table 1. Fluorescent lamp synthetic apatite phosphors.

Composition	****Emission color***	***Emission peak(s)***	***Application***
$3Ca_3(PO_4)_2\ Ca(F,Cl)_2:Sb^{3+}$	blue white	480	Fl lamps
$^{\S}3Ca_3(PO_4)_2\ Ca(F,Cl)_2:Sb^{3+},Mn^{2+}$	daylight	480, 575	Fl lamps
$^{\S}3Ca_3(PO_4)_2\ Ca(F,Cl)_2:Sb^{3+},Mn^{2+}$	white	480, 575	Fl lamps
$^{\S}3Ca_3(PO_4)_2\ Ca(F,Cl)_2:Sb^{3+},Mn^{2+}$	warm white	480, 580	Fl lamps
$Sr_{10}(PO_4)_6\ Cl_2:Eu^{2+}$	blue	447	Three-band and high-pressure lamps
$(Sr,Ca)_{10}(PO_4)_6\ Cl_2:Eu^{2+}$	blue	452	Three-band lamps
$(Sr,Ca)_{10}(PO_4)_6\ nB_2O_3:Eu^{2+}$	blue	452	Three-band lamps
$(Sr,Ca,Mg)_{10}(PO_4)_6\ Cl_2:Eu^{2+}$	blue-green	483	Color reproduction
$(Sr,Ca,Ba)_{10}(PO_4)_6\ Cl_2:Eu^{2+}$	blue	445	Color reproduction
$(Ba,Ca,Mg)_{10}(PO_4)_6\ Cl_2:Eu^{2+}$	varies with Ba/Ca ratio		Color reproduction

*Industry trade names

§Variable concentrations of Sb^{3+} and Mn^{2+} amongst the three formulas.

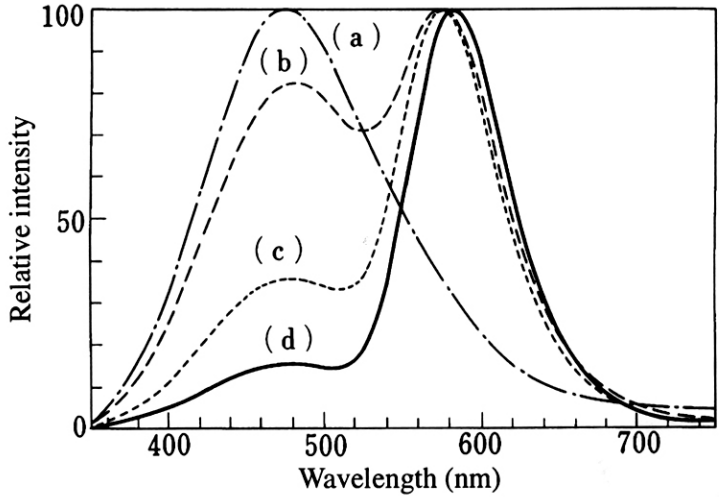

Figure 28. Comparison of halophosphate phosphor emission spectra. Modified after Shionoya and Yen (1999).

(a) Blue-white. Ratio of $Mn^{2+}:Sb^{3+} = 0:0.15$,

(b) Daylight 0.08:0.08,

(c) Cool-white 0.17:0.08,

(d) Warm-white 0.24:0.08.

halophosphor. The white colors noted in Table 1 can be referred to temperatures for a black body emitter obeying Plank's law. In this scheme, white is equivalent to black body emission at 3500 K, while warm white is equivalent to emission at 3000 K. "Cooler" light richer in blue would be produced at higher black body temperatures. High-pressure Hg lamps require another type of lamp phosphor. This Hg discharge has increased emission at 365 nm relative to the low-pressure standard fluorescent lamp, so the phosphor must absorb both SWUV and LWUV (= UVC and UVA) to efficiently produce white light. In such high-pressure lamps, the operational temperature is in the range of 600 K, so the phosphor must have a very high threshold for thermal quenching. Under these conditions Sr chlorapatite doped with Eu^{2+} operates well, but other halophosphors do not perform as well as Eu^{3+} and Tb^{3+} activated oxide phosphors.

Laser applications

Fluorapatites have been examined fairly extensively as CW laser host crystals since the discovery by Ohlmann et al. (1968) that Nd^{3+} activated fluorapatite had much higher gain and efficiency than any other Nd^{3+} host. The excellent laser properties are due to the very sharp 1060 nm emission band and the broad absorption spectrum within the large band gap. Unfortunately, these advantages are not enough to overcome the low thermal conductivity of fluorapatite, which causes build up of temperature and crystal distortion even at low power outputs. Additionally, problems existed in the preparation of large optical grade crystals of fluorapatite. Thus other apatite compositions and other dopants have been examined to explore ways to improve thermal conductivity or reduce emission bandwidth. Steinbruegge et al. (1972) examined Nd^{3+}, Ho^{3+} and Tm^{3+} doped Ca, Mg, Sr and Ba fluorapatite, CaLa oxyapatite, and CaY, CaLa and SrLa silicate apatite. The silicate oxyapatites could accommodate more REE than the phosphate apatites, as well as REE of either trivalent or divalent charge, and had fluorescence line widths about ten times broader than in fluorapatite. They are also harder and more thermal shock resistant than Nd^{3+}doped fluorapatite, and could be grown into high quality large crystals without difficulty.

With the advent of diode laser pumping it became practical to use fluorapatite once again as a laser host for Nd^{3+} because the crystal size could be markedly reduced and thus the thermal load decreased. Zhang et al. (1994) prepared such small fluorapatite crystals and demonstrated diode pumped lasing action with high efficiency. Another set of apatite laser hosts were explored by Payne et al. (1994a) using Yb-doped Ca, Sr, and CaSr fluorapatites, and Sr vanadate apatite. Yb^{3+} is a useful laser dopant species in YAG, but is limited due to the paucity of available absorption transitions for pumping using flash lamps and other undirected excitation methods. As with Nd^{3+} doped fluorapatite, this difficulty was also solved by the use of semiconductor diode lasers as pumps, as they can be made to produce directed excitation beams with narrow emission band widths. One way to measure laser materials utility is via a plot of the absorption cross section versus the minimum pump saturation intensity, i.e., the minimum pump intensity needed to reach laser action. Such a plot is shown in Figure 29, and shows the favorable location of the Yb^{3+}-doped apatites prepared by Payne et al. (1994a).

Another approach in apatite structure laser hosts is that by Scott et al. (1997) using $3d^2$ ions substituted into the phosphate sites of Ca fluorapatite and Sr vanadate apatite. In Ca fluorapatite, Cr^{4+} substitution required that one of the tetrahedral ligand oxygens be replaced by fluorine for charge compensation, which causes inhomogeneous broadening of the spectral bands. There is no analogous problem for Mn^{5+} substitution, and $Sr_{10}(VO_4)_6F_2$:Mn^{5+} showed ideal laser characteristics with emission at 1160 nm. Mn^{5+} doped into Sr fluorapatite and other phosphates for laser applications has also been examined by Copobianco et al. (1992), and the luminescence properties of Mn^{5+} in a

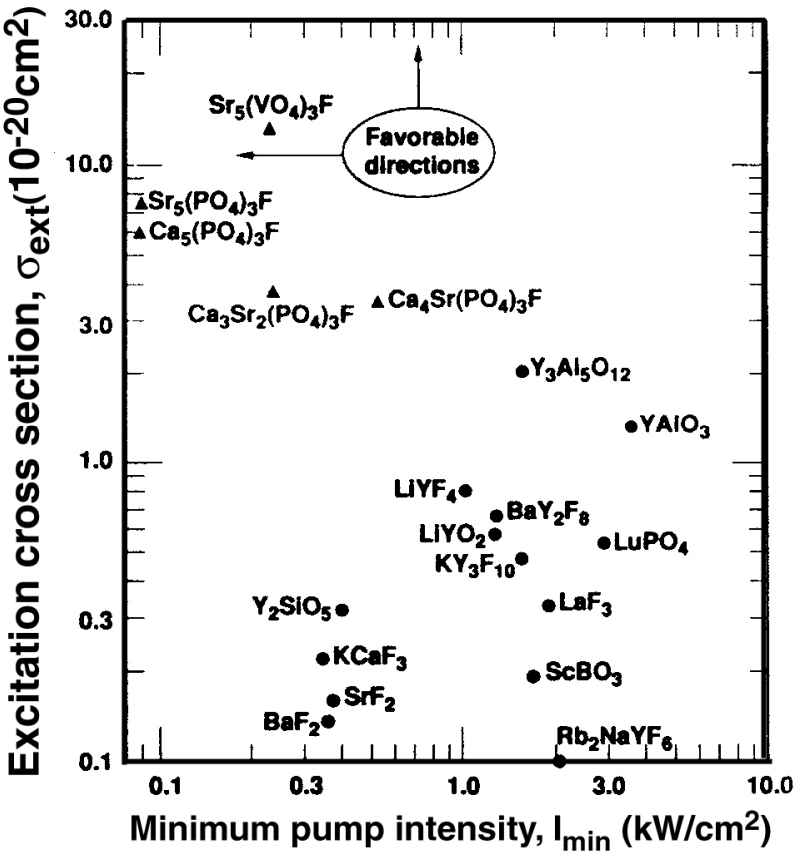

Figure 29. Laser performance parameter chart. Modified after Payne et al. (1994).

variety of apatite structures has been described by Oetliker et al. (1994). The latter work indicates very low thermal quenching at room temperature in the apatite structures compared to other Mn^{5+} host crystals, a distinct advantage for laser applications.

ISSUES CONCERNING APATITE LUMINESCENCE

Apatite luminescence is sufficiently complex that very many questions remain about activators, energy transfer, quenching effects, and site occupation. Although the crystal chemistry of fluorapatite is fairly well understood, the same cannot be said for many of the other apatite compositions with respect to activator placement, charge compensation, defect structures and lattice effects on luminescent properties. Outstanding questions also remain on the possible use of apatite luminescence for age dating or paleotemperature measurements, as the thermoluminescence behavior has had limited investigation. On the other hand, progress has been made in understanding the history of growth of apatites via luminescence mapping to yield REE selective uptake and redox information. With the continued development of micro CL methods (e.g., Kempe and Gotze 2002) a potentially powerful complementary tool is added to standard microprobe or SEM chemical analysis (Fig. 30). Quantitative measurement of REE concentration levels in apatite group minerals via luminescence spectroscopy, which is plagued by energy transfer issues in CL and UV-excited work, might be practically done using time-resolved laser-excitation techniques. This can potentially also be extended to microfocus situations and even raster-scanning of samples given adequate laser focusing and detector speed. Such capabilities depend on the ability to excite directly into the particular REE excitation bands, and measure emission before energy transfer has occurred. This may be possible

for many of the REE, allowing improved feasibility for REE partitioning measurements at extremely low REE concentrations, and the use of REE relative abundance signatures to extract information on petrologic history. For the mineral collector who appreciates apatite luminescence, there seems to be almost no end to the diversity of natural materials which have been located, and are being newly discovered. With the advent of UV tunable lasers in the not so distant future, many of these enthusiasts will be turned into amateur spectroscopists by this single species.

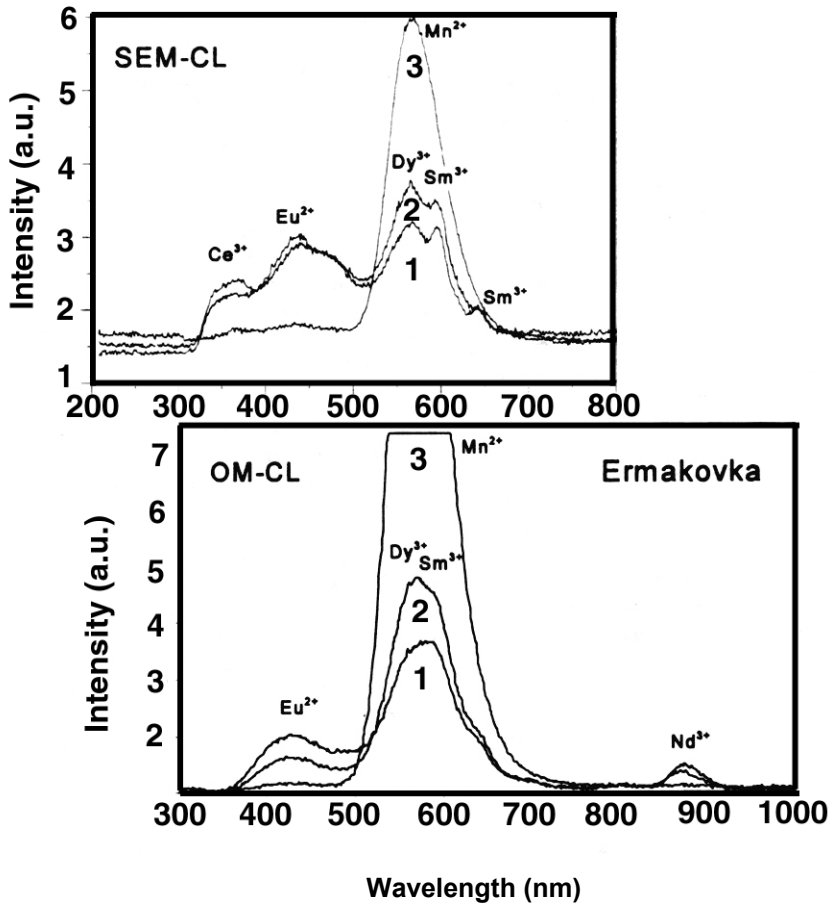

Figure 30. Micro (SEM) vs. bulk (optical microscope apparatus) CL from a sample of fluorapatite from a Be deposit at Ermakova, Russia. The numbers refer to positions on the crystal. 3 is near the crystal rim, while 1 and 2 are in the interior. Modified after Kempe and Götze (2002).

ACKNOWLEDGMENTS

Past discussions with Emmanuel Fritsche, Manuel Robbins, John Rakovan and many members of the Fluorescent Mineral Society (FMS) both contributed to and inspired this chapter. Thorough reviews by John Hanchar, John Rakovan, Will White and George Rossman contributed substantially to the final composition, and they are much appreciated. Manuscript and figure production was assisted by the staff of the Geochemistry department at the Lawrence Berkeley National Laboratory. Support for the this work came from the Office of Science, Office of Basic Energy Sciences, Division of Chemical Sciences, Geosciences Research Program of the U.S. Department of Energy under contract DE-AC03-76-SF00098 to LBNL.

REFERENCES

Al-Khalifa IJM, James K, Durrani SA, Khalifa MS (1988) Radiation damage studies of mineral apatite, using fission tracks and thermoluminescence techniques. Nucl Tracks Rad Measure 15:61-64

Barbarand J, Pagel M (2001) Cathodoluminescence study of apatite crystals. Am Mineral 86:473-484

Baumer A, Lapraz D, Klee WE (1987) Thermoluminescent properties of hydrothermally prepared apatites. Neues Jahrb Mineral Mon 1987:43-48

Benoit PH, Sears DWG (1997) The orbits of meteorites from natural thermoluminescence. Icarus 125: 281-287

Benoit PH, Sears DWG (1991) The natural thermoluminescence of meteorites. II. Meteorite orbits and orbital evolution. Icarus 94:311-325

Blanc P, Baumer A, Cesbron F, Ohnenstetter D (1995) Les activateurs de Cathodoluminescence dans les chlorapatites preparees par synthese hydrothermale. C R Acad Sci Paris Ser IIa 321:119-126

Blanc P, Baumer F, Cesbron F, Ohnenstetter D, Panczer G, Remond G (2000) Systematic cathodoluminescence spectral analysis of synthetic doped minerals: Anhydrite, apatite, calcite, fluorite, scheelite and zircon. *In* Cathodoluminescence in Geosciences. Pagel M, Barbin V, Blanc P, Ohnenstetter D (eds) Springer Verlag, Berlin

Blasse G, Bleijenberg KC, Krol DM (1979) The luminescence of hexavalent uranium in solids. J Lumin 18-19:57-62

Blasse G (1988) Luminescence of inorganic solids: From isolated centers to concentrated systems. Prog Sol State Chem 18:79-191

Blasse G, Aguilar M. (1984) Luminescence of natural calcite ($CaCO_3$). J Lumin 29:239-241

Blasse G, Bril A (1967) Investigation of Ce^{3+}-activated phosphors. J Chem Phys 47:5139-5145

Blasse G, Grabmaier BC (1994) Luminescent Materials. Springer-Verlag, Berlin

Bostwick RC (1977) The fluorescent minerals of Franklin and Sterling Hill. J Fluor Mineral Soc 6:7-40

Botden TPJ, Kröger FA (1948) Energy transfer in sensitized $Ca_3(PO_4)_2$:Ce:Mn and $CaSiO_3$:Pb:Mn. Physica 14:553-566

Burns RG (1993) Mineralogical Applications of Crystal Field Theory. Cambridge University Press, Cambridge, UK

Chen N, Pan Y, Weil JA (2002a) Electron paramagnetic resonance study of synthetic fluorapatite: Part 1. Local structural environment and substitution mechanism of Gd^{3+} at the Ca2 site. Am Mineral 87: 37-46

Chen N, Pan Y, Weil JA, Nilges MJ (2002b) Electron paramagnetic resonance study of synthetic fluorapatite: Part 2. Gd^{3+} at the Ca1 site, with a neighboring Ca1 vacancy. Am Mineral 87:47-55

Chenot CF, Kasenga AF, Poppalardo RE. (1981) Depreciation in cerium-activated fluorapatite phosphors. J Lumin 24-25:95-98

Copobianco JA, Cormier G, Moncourge R, Manaa H, Bertinelli M. (1992) Gain measurements of Mn^{5+} ($3d^2$) doped $Sr_5(PO_4)_3Cl$ and Ca_2PO_4Cl. Appl Phys Lett 60:163-165

Cotton FA (1971) Chemical Applications of Crystal Field Theory. John Wiley & Sons, New York

Cotton FA, Wilkinson G (1980) Advanced Inorganic Chemistry, 5th Edition. John Wiley & Sons, New York

DeBoer BG, Sakthivel A, Cagle JR, Young RA (1991) Determination of the antimony substitution site in calcium fluorapatite from powder x-ray diffraction data. Acta Crystallogr B 47:683-692

DeLoach LD, Payne SA, Kway WL, Tasssano JB, Dixit SN, Krupke WF (1994) Vibrational structure in the emission spectrum of Yb(3+) doped apatite crystals. J Lumin 62:85-94

DeNeufville JP, Kasdan A, Chimenti R (1981) Selective detection of uranium by laser-induced fluorescence: A potential remote sensing technique. I. Optical characteristics of uranyl geologic targets. Appl Optics 20:1279-1296

Diaz MA, Luff BJ, Townsned PD, Wirth KR (1991) Temperature dependence of luminescence from zircon, calcite, iceland spar and apatite. Nucl Tracks Rad Measure 18:45-51

Elliott JC (1994) Structure and Chemistry of the Apatites and Other Calcium Orthophosphates. Elsevier, Amsterdam, The Netherlands

Filippelli GM, Delaney ML (1993) The effect of manganese (II) and iron (II) on the cathodoluminescence signal in synthetic apatite. J Sed Petrol 63:167-173

Fleet ME, Pan Y (1994) Site preference of Nd in fluorapatite ($Ca_{10}(PO_4)_6F_2$). J Solid State Chem 112:78-81

Fleet ME, Pan Y (1995a) Crystal chemistry of rare earth elements in fluorapatite and some calc-silicates. Eur J Mineral 7:591-605

Fleet ME, Pan Y (1995b) Site preference of rare earth elements in fluorapatite. Am Mineral 80:329-335

Fleet ME, Pan Y (1997a) Site preference of rare earth elements in fluorapatite: Binary (LREE+HREE)-substituted crystals. Am Mineral 82:870-877

Fleet ME, Pan Y (1997b) rare earth elements in apatite: Uptake from H_2O-bearing phosphate-fluoride melts and the role of volatile components. Geochim Cosmochim Acta 61:4745-4760

Gaft M, Bershov L, Krasnaya A, Yaskolko V (1985) Luminescence centers in anhydrite, barite, celestite and their synthesized analogs. Phys Chem Minerals 11:255-260

Gaft M, Reisfeld R, Panczer G, Shoval S, Garapon C, Boulon G, Strek W (1996a) Luminescence of Eu(III), Pr(III) and Sm (III) in carbonate-fluor-apatite. Acta Phys Pol A 90:267-274

Gaft M, Shoval S, Panczer G, Nathan Y, Champagnon B, Garapon C (1996b) Luminescence of uranium and rare-earth elements in apatite of fossil fish teeth. Palaeogeogr Palaeoclimatol Palaeoecol 126: 187-193

Gaft M, Reisfeld R, Panczer G, Shoval S, Champagnon B, Boulon G (1997a) Eu^{3+} luminescence in high-symmetry sites of natural apatite. J Lumin 72:572-574

Gaft M, Reisfeld R, Panczer G, Boulon G, Shoval S, Champagnon B (1997b) Accommodation of rare-earths and manganese by apatite. Opt Materials 8:149-156

Gaft M, Reisfeld R, Panczer G, Blank P, Boulon G (1998a) Laser-induced time-resolved luminescence of minerals. Spectrochim Acta A 54:2163-2175

Gaft M, Reisfeld R, Panczer G, Uspensky E, Varrel B, Boulon G (1999) Luminescence of Pr^{3+} in minerals. Opt Materials 13:71-79

Gaft M, Panczer G, Reisfeld R, Shinno I, Champagnon B, Boulon G (2000) Laser-induced Eu^{3+} luminescence in zircon $ZrSiO_4$. J Lumin 87-89:1032-1035

Gaft M, Panczer G, Reisfeld R, Uspensky E (2001a) Laser-induced time-resolved luminescence as a tool for rare-earth element identification in minerals. Phys Chem Minerals 28:347-363

Gaft M, Reisfeld R, Panczer G, Ioffe O, Sigal I (2001b) Laser-induced time-resolved luminescence as a means for discrimination of oxidation states of Eu in minerals. J Alloys Compounds 323-324:842-846

Gait RI, Back ME (1992) Pyromorphite: A review. Rocks Minerals 67:22-36

Garcia J, Sibley WA (1988) Energy transfer between europium and manganese ions. J Lumin 42:109-116

Garlick GFJ (1958) *In* Handbook der Physik. Vol XXVI. Flugge S (ed) Springer, Berlin–Heidelberg–New York, p 1

Gorobets BS (1968) On the luminescence of fluorapatite activated by rare-earth elements. Optics Spectr 25:154-155

Gorobets BS (1981) Luminescence Spectra of Minerals. (in Russian) Moscow. 153 p

Gotze J, Heimann RB, Hildebrandt H, Gburek U (2001) Microstructural investigation into calcium phosphate biominerals by spatially resolved cathodoluminescence. Mater Wissen Werkstofftechnik 32:130-136

Grandjean-Lecuyer P, Feist R, Albarede, F (1993) Rare-earth elements in old biogenic apatites. Geochim Cosmochim Acta 57:2507-2514

Gruber JB, Wright AO, Seltzer MD, Zandi B, Merkle LD, Hutchinson JA, Morrison CA, Allik TH, Chai BHT (1997a) Site-selective excitation and polarized absorption and emission spectra of trivalent thulium and erbium in strontium fluorapatite. J Appl Phys 81:6585-6598

Gruber JB, Zandi B, Seltzer MD (1997b) Spectra and energy levels of trivalent holmium in strontium fluorapatite. J Appl Phys 81:7506-7513

Gruber JB, Zandi B, Merkle L (1998) Crystal-field splitting of energy levels of rare earth ions $Dy^{3+}(4f^9)$ and $Yb^{3+}(4f^{13})$ in M(II) sites in fluorapatite crystal $Sr_5(PO_4)_3F$. J Appl Phys 83:1009-1016

Gruber JB, Zandi B, Ferry M, Merkle L (1999) Spectra and energy levels of trivalent samarium in strontium fluorapatite. J Appl Phys 86:4377-4382

Guimon RK, Weeks KS, Keck BD, Sears DWG (1984) Thermoluminescence as a paleothermometer. Nature 311:363-365

Habermann D, Gotte T, Meijer J, Stephan A, Richter DK, Niklas JR (2000) High-resolution rare-earth element analyses of natural apatite and its applications in geo-sciences: Combined micro-PIXE, quantitative CL spectroscopy and electron spin resonance analyses. Nucl Inst Methods Phys Res B 161-163:846-851

Henderson B, Imbusch GF (1989) Optical Spectroscopy of Inorganic Solids. Clarendon Press, Oxford

Henkel G (1989) The Henkel glossary of fluorescent minerals. Verbeek E, Modreski P (eds) *In* J Fluor Mineral Soc, Vol. 15

Hughes JM, Cameron M, Crowley KD (1991a) Ordering of the divalent cations in the apatite structure: Crystal structure refinements of natural Mn- and Sr-bearing apatite. Am Mineral 76:1857-1862

Hughes JM, Cameron M, Mariano AN (1991b) Rare-earth-element ordering and structural variations in natural rare-earth-bearing apatites. Am Mineral 76:1165-1173

Jagannathan R, Kottaisamy M. (1995) Eu^{3+} luminescence: A spectral probe in $M_5(PO_4)_3X$ apatites (M = Ca or Sr, X = F^-, Cl^-, Br^- or OH^-. J Phys Condens Matter 7:8453-8466

Jagannathan R, Kutty TRN (1997) Anomalous fluorescence features of Eu^{2+} in apatite-pyromorphite type matrices. J Lumin 71:115-121

Jenkins HG, McKearg AH, Ranby PW (1949) Alkaline earth halophosphates and related phosphors. J Electrochem Soc 96:1-12

Kalsbeek N, Larsen S, Ronsbo JG (1990) Crystal structures of rare earth elements rich apatite analogues. Z Kristallogr 191:249-263

Kempe J, Gotze J (2002) Cathodoluminescence (CL) behavior and crystal chemistry of apatite from rare-metal deposits. Mineral Mag 66:151-172

Knutson C, Peacor DR, Kelly WC (1985) Luminescence, color and fission track zoning in apatite crystals of the Panasqueira tin-tungsten deposit, Beira-Baixa, Portugal. Am Mineral 70:829-837

Kottaisamy M, Jagannathan R, Jeyagopal P, Rao RP, Narayanan R (1994) Eu^{2+} luminescence in $M_5(PO_4)_3X$ apatites, where M is Ca^{2+}, Sr^{2+} and Ba^{2+}, and X is F^-, Cl^-, Br^- and OH^-. J Phys D 27:2210-2215

Lapraz D, Baumer A (1983) Thermoluminescent properties of synthetic and natural fluorapatite, $Ca_5(PO_4)3_F$. Phys Stat Solidi A 80:353-366

Lapraz D, Gaume F, Barland M (1985) On the thermoluminescent mechanism of a calcium fluorapatite single crystal doped with Mn^{2+}. Phys Stat Solidi A 89:249-253

Leckebusch R (1979) Comments on the luminescence of apatites from Panasqueria (Portugal). N Jahrb Mineral Monat 17-21

Leverenz HW (1968) An Introduction to Luminescence of Solids. Dover Publications, New York

Louis-Achille V, DeWindt L, Defranceschi M (2000) Electronic structure of minerals: The apatite group as a relevant example. Intl J Quantum Chem. 77:991-1006

Loutts GB, Hong P, Chai BHT (1994) Comparison of neodymium laser hosts based on a fluoro-apatite structure. Mater Res Soc 1994:45-49

Mackie PE, Young RA (1973) Location of Nd dopant in fluorapatite, $Ca_5(PO_4)_3F$:Nd. J Appl Crystallogr 6:26-31

Marfunin AS (1979) Spectroscopy, Luminescence and Radiation Centers in Minerals. Springer-Verlag, Berlin

Mariano AN (1988) Some further geological applications of cathodoluminescence. *In* Cathodoluminescence of Geological Materials. Marshall DJ (ed) Unwin Hyman, Boston

Mariano AN (1989) Cathodoluminescence emission spectra of REE activators in minerals. Rev Mineral 21:339-348

Mariano AN, Ring PJ (1975) Europium-activated cathodoluminescence in minerals. Geochim Cosmochim Acta 39:649-660

Marshall DJ (1988) Cathodoluminescence of Geologic Materials. Unwin Hyman, Boston, 146 p

Mayer I, Layani JD, Givan A, Gaft M, Blanc P (1999) La ions in precipitated hydroxyapatites. J Inorg Biochem 73:221-226

McConnel D (1973) Apatite: Its crystal chemistry, mineralogy, utilization, and geologic and biologic occurrences. Applied Mineralogy 5. Springer-Verlag, New York

McKeever SWS (1985) Thermoluminescence of Solids. Cambridge University Press, Cambridge, UK

McKeever SWS, Sears DW (1979) Meteorites and Thermoluminescence. Meteoritics 14:29-41

Mitchell RH, Xiong J, Mariano AN, Fleet ME (1997) Rare-earth-element-activated cathodoluminescence in apatite. Can Mineral 35:979-998

Moncorge R, Manaa H, Boulon G (1994) Cr^{4+} and Mn^{5+} active centers for new solid state laser materials. Opt Mater 4:139-151

Moran LB, Berkowitz JK, Yesinowski JP (1992) ^{19}F and ^{31}P magic-angle spinning nuclear magnetic resonance of antimony (III)-doped fluorapatite phosphors: Dopant sites and spin diffusion. Phys Rev B 45:5347-5360

Morozov A, Morozova L, Trefilov A, Feofilov P (1970) Spectral and luminescent characteristics of fluorapatite single crystals activated by rare earth ions. Opt Spectros 29:590-596

Murray JR, Oreskes N (1997) Uses and limitations of cathodoluminescence in the study of apatite paragenesis. Econ Geol 92:368-376

Narita K (1961) Energy spectrum of Mn^{++} ion in Calcium Fluorophosphate. I. J Phys Soc Japan 16:99-105

Narita K (1963) Energy spectrum of Mn^{++} ion in Calcium Fluorophosphate. II. J Phys Soc Japan 18:79-86

Nor AF, Amin YM, Mahat R, Kamaluddin B (1994) Thermoluminescence of Apatite. Solid State Sci Tech 2:294-300

Oetliker U, Herren M, Gugel HU, Kesper U, Albrecht C, Reinen D (1994) Luminescence properties of Mn^{5+} in a variety of host lattices: Effects of chemical and structural variation. J Chem Phys 100: 8656-8665

Ohlmann RC, Steinbruegge KB, Maczelsky R (1968) Spectroscopic and laser characteristics of neodymium-doped calcium fluorophosphate. Appl Opt 7:905-914

Oomen EWJL, Smit WMA, Blasse G (1988) Luminescence of the Sb^{3+} ion in calcium fluorapatite and other phosphates. Mater Chem Phys 19:357-368

Palilla FC, O'Reilly BE (1968) Alkaline-earth halophosphate phosphors activated by divalent europium. J Electrochem Soc 115:1076-1081

Panczer G, Gaft M, Reisfeld R, Shoval S, Boulon G, Champagnon B (1998) Luminescence of uranium in natural apatites. J. Alloys Compounds 275-277:269-272

Payne SA, DeLoach LD, Smith LK, Kway WL, Tassno JB, Krupke WF, Chai BHT, Loutts G (1994a) Ytterbium-doped apatite-structure crystals-a new class of laser materials. J Appl Phys 76:497-503

Payne SA, Smith LK, DeLoach LD, Kway WL, Tassano JB, Krupke WF (1994b) Laser, optical, and thermomechanical properties of Yb-doped fluorapatite. IEEE J Quantum Elect 30:170-179

Perseil E-A, Blanc P, Ohnenstetter D (2000) As-bearing fluorapatite in manganiferous deposits from St. Marcel-Praborna, Val D'Aosta, Italy. Can Mineral 38:101-117

Piriou B, Elfakir A, Quarton M (2001) Site-selective spectroscopy of Eu^{3+}-doped sodium lead phosphate apatite. J Lumin 93:17-26

Portnov AM, Gorobets BS (1969) Luminecence of apatite from different rock types. Dokl Akad Nauk SSSR 184:110-115 (in Russian)

Rakavon J, Hughes JM (2000) Strontium in the apatite structure: Strontian apatite and belovite-Ce. Can Mineral 38:839-845

Rakovan J, Reeder RJ (1994) Differential incorporation of trace elements and dissymmetrization in apatite: The role of surface structure during growth. Am Mineral 79:892-903

Rakovan J, Reeder RJ (1996) Intracrystalline rare earth element distributions in apatite:
Surface structural influences on zoning during growth. Geochem. Cosmochim. Acta 60:4435-4445

Rakovan J, Waychunas GA (1996) Luminescence in minerals. Mineral Record 27:7-19

Rakovan J, McDaniel DK, Reeder RJ (1997) Use of surface-controlled REE sectoral zoning in apatite from Llallagua, Bolivia, to determine a single crystal Sm-Nd age. Earth Planet Sci Lett 146:329-336

Rakovan J, Newville M, Sutton S (2001) Evidence of Heterovalent Europium in Zoned Llallagua Apatite using Wavelength Dispersive XANES. Am Mineral 86:697-700

Ramesh R, Jagannathan R (2000) Optical properties of Ce^{3+} in self-assembled strontium chloro-(hydroxyl)apatite nanocrystals. J Phys Chem B 104:8351-8360

Ratnam VV, Jayaprakish R, Daw NP (1980) Thermoluminescence and thermoluminescence spectra of synthetic fluorapatite. J Lumin 21:417-424

Reisfeld R, Gaft M, Boulon G, Panczer C, Jrgensen CK (1996) Laser-induced luminescence of rare-earth elements in natural fluor-apatites. J Lumin 69:343-353

Remond G, Cesbron F, Chapoulie R, Ohnenstetter D, Roques-Carmes C, Schvoerer M (1992) Cathodoluminescence applied to microcharacterization of mineral materials: The present status in experimentation and interpretation. Scanning Micros 6:23-68

Robbins DJ (1980) On predicting the maximum efficiency of phosphor systems excited by ionizing radiation. J Electrochem Soc 127:2694-2701

Robbins M (1983) The collectors book of fluorescent minerals. Van Nostrand Reinhold, New York

Robbins M (1994) Fluorescence: Gems and Minerals Under Ultraviolet Light. Geoscience Press, Phoenix

Roeder PL, MacArthur D, Ma X-P, Palmer GR, Mariano AN (1987) Cathodoluminescence and microprobe study of rare-earth elements in apatite. Am Mineral 72:801-811

Ronsbo JG (1989) Coupled substitutions involving REEs and Na and Si in apatites in alkaline rocks from the Ilimaussaq intrusion, South Greenland, and the petrological implications. Am Mineral 74:896-901

Ropp RC (1971) The emission colors of the strontium apatite phosphor system. J Electrochem Soc 118:1510-1512

Rossman GR (1988) Optical Spectroscopy. Rev Mineral 18:207-254

Ryan FM, Vodoklys FM (1971) The Optical Properties of Mn^{2+} in Calcium halophosphate phosphors. J Electrchem Soc 118:1814-1819

Ryan FM, Ohlmann RC, Murphy J, Mazelsky R, Wagner GR, Warren RW (1970) Optical properties of divalent manganese in calcium fluorophosphate. Phys Rev B 2:2341-2352

Scott MA, Han TPJ, Gallagher HG, Henderon B (1997) Near-infrared laser crystals based on $3d^2$ ions: Spectroscopic studies of $3d^2$ ions in oxide, melilite and apatite crystals. J Lumin 72-74:260-262

Sears DWG (1980) Thermoluminescence of meteorites: Relationships with their K-Ar age and their shock and reheating history. Icarus 44:190-206

Shionoya S, Yen WM (1999) Phosphor Handbook. CRC Press, Boca Raton, Florida

Smith JV, Stenstrom RC (1965) Electron-excited luminescence as a petrologic tool. J Geol 73:627-635

Stefanos SM, Bonner CE, Meegoda C, Rodriguez WJ, Loutts GB (2000) Energy levels and optical properties of neodymium-doped barium fluorapatite. J Appl Phys 88:1935-1942

Solomonov VI, Osipov VV, Mikhailov SG (1993) Pulse-periodic cathodoluminescence of apatite. Zh Prikladnoi Spectroskopii 59:107-113

Steinbruegge KB, Hennigsen T, Hopkins RH, Mazelsky R, Melamed NT, Riedel EP, Roland GW (1972) Laser properties of Nd^{3+} and Ho^{3+} doped crystals with the apatite structure. Appl Optics 11:999-1012

Stokes GG (1852) On the change of refrangibility of light. Phil Trans 142:463-562

Suitch PR, LaCout JL, Hewat A, Young RA (1985) The structural location and role of Mn^{2+} partially substituted for Ca^{2+} in fluorapatite. Acta Crystallogr B41:173-179

Tachihante M, Zambon D, Cousseins JC (1996) optical study of the Tb^{3+} to Eu^{3+} energy transfer in calcium fluorapatite. Eur J Solid State Inorg Chem 33:713-725

Taraschan A. (1978) Luminescence of Minerals. Naukova Dumka, Kiev (in Russian)

Taraschan A, Waychunas G (1995) Luminescence of minerals. *In* Advanced Mineralogy 2. Methods and Instrumentation. Marfunin A (ed) Springer, Berlin, p 124-135

Ternane R, Trabelsi-Ayedi M, Kbir-Ariguib N, Piriou B (1999) Luminescent properties of Eu in calcium hydroxyapatite. J Lumin 81:153-236

Vasilenko VB, Sotnikov VI, Nikitina YI, Kholodova LD (1968) The possibility of using apatite luminescence in geologic thermometry (in Russian). Geologiya Geofizika 11:131-135

Voronko YK, Gorbachev AV, Zverev AA, Sobil AA, Morozov NN, Muravev EN, Niyazov SA, Orlovskii VP (1992) Raman scattering and luminescence spectra of compounds with the structure of apatite $Ca_5(PO_4)_3F$ and $Ca_5(PO_4)_3OH$ activated with Eu^{3+} ions. Inorg Mater 28:442-447

Voronko YK, Maksimova G, Sobol AA (1991) Anisotropic luminescence centers of TR^{3+} ions in fluorapatite crystals. Opt Spectros 70:203-206

Wachtel A (1958) The effect of impurities on the plaque brightness of a 3000 K calcium halophosphate phosphor. J Electrochem Soc 105:256-260

Warren RW (1970) EPR of Mn^{2+} in calcium fluorophosphates. I. The Ca (II) site. Phys Rev B 2:4383-4388

Waychunas G (1989) Luminescence, X-ray emission and new spectroscopies. Rev Mineral 18:638-698

Wright AO, Seltzer MD, Gruber JB, Zandi B, Merkle LD, Chai BHT (1996) Spectroscopic investigation of Pr^{3+} in fluorapatite crystals. J Phys Chem Solids 57:1337-1350

Xiong J (1995) Cathodoluminescence studies of feldspars and apatites from the Coldwell alkaline complex. MSc thesis, Lakehead Univ, Thunder Bay, Ontario

Zhang XX, Loutts GB, Bass M, Chai BHT (1994) Growth of laser-quality single crystals of Nd^{3+}-doped calcium fluorapatite and their efficient lasing performance. Appl Phys Lett 64:10-12